Deterioration of stone and concrete exposed to bird excreta – examination of the role of glyoxylic acid

Dyer, Thomas

Published in:
International Biodeterioration and Biodegradation

DOI:
10.1016/j.ibiod.2017.09.002

Publication date:
2017

Document Version
Peer reviewed version

Deterioration of stone and concrete exposed to bird excreta – examination of the role of glyoxylic acid.

Thomas Dyer

Concrete Technology Unit

University of Dundee

Dundee

UK

DD1 4HN

t.d.dyer@dundee.ac.uk

ABSTRACT: The deterioration of buildings as a result of the deposition of bird excreta is a phenomenon which has been well-documented. A number of mechanisms have been proposed as playing a role in deterioration, some of which involve biological processes. Uric acid in bird excreta is broken down by fungi into urea and glyoxylic acid. This paper examines the effect of exposing stone and cement specimens to glyoxylic acid solutions. These materials were a limestone, a sandstone and two cement pastes – Portland and calcium sulfoaluminate cement. Specimens of these materials were submerged in acid solutions and deterioration characterised using mass loss measurements, micro-CT scanning, and analysis of the solutions at the end of the experiment and the acid-degraded layers at the specimen surface. Attempts were made to synthesise and characterise calcium salts of glyoxylic acid. Additionally, geochemical modelling was conducted to provide further understanding of the deterioration processes. The results indicate that the main processes involved in glyoxylic acid attack of the materials investigated are acidolysis and complex formation. No calcium glyoxylate salts were present in the degraded materials. Instead, a conversion of glyoxylate to oxalate occurred leading to precipitation of calcium oxalate compounds.

KEYWORDS

bird excreta; fungi; glyoxylic acid; limestone; sandstone; cement.

1. INTRODUCTION

The deposition of bird excreta possesses the potential to initiate biodeterioration of the fabric of buildings through a number of routes (Spennemann et al. 2017). Mechanisms include the enlargement of cracks and joints by vascular plants deriving from seeds in the excreta (Lisci et al. 2003), and damage from its chemical constituents. Additionally, bird excreta may act as a source of nutrients to micro-organisms, which may lead to biodeterioration through the production of metabolites.

Bird excreta consists of two components – urine and faeces - which are usually voided simultaneously. Urine largely takes the form of fine crystals of uric acid dihydrate ($C_5H_4N_4O_3.2H_2O$) dispersed in a small volume of water. Depending on the species of bird, other nitrogen-bearing substances may be present, including urea, ammonium compounds, purines, creatine, creatinine and amino acids (Bernardi et al. 2009). The faecal matter contains the residue of organic material ingested by the bird. It may also contain fragments of inorganic minerals – 'grit' - ingested to aid in the digestion of seed and grain (Gómez-Heras et al. 2004). One study identified other insoluble salts – specifically members of the apatite group ($Ca_{10}(PO_4)_6(OH,F,Cl)_2$) and calcium oxalate (Gómez-Heras et al. 2004). A number of soluble salts were also present: halite (NaCl), sylvite (KCl), aphthitalite ($(Ka,Na)_3Na(SO_4)_2$), and calcium langbeinite ($Ca_2K_2(SO_4)_3$). These salts were present in relatively small quantities.

Uric acid is almost insoluble and so its capacity for causing damage through acidolysis is limited. Whilst it has been observed that repeated dissolution and re-precipitation of uric acid from bird excreta on building surfaces can lead to staining (Haag-Wackernagel 2012), most studies conclude that it does not lead directly to physical damage (Hempel and Moncrieff 1971; Del Monte 1986). However, crystallisation pressures exerted by soluble salt constituents during cyclical wetting and drying have been attributed to deterioration of tuffs in the Midas monument in Turkey (Topal and Sözmen 2003).

Many microorganisms are capable of using uric acid as a source of nitrogen. In particular, fungi degrade uric acid via the pathway:

Uric acid → Allantoin → Allantoic acid → Ureidoglycolic acid → Glyoxylic acid + Urea

(Vogels and Van der Drift 1976; Vera-Ponce de Leon et al. 2016)

Vogels and Van der Drift (1976) have compiled a list of fungal species found to able to use uric acid. From this, the species identified in the literature as having been isolated from bird excreta are the microfungus *Microascus brevicaulis*, as well as the filamentous fungi *Penicillium chrysogenum*, *Aspergillus fumigatus*, *A. niger* and *Beauveria bassiana*.

A study examining damage resulting from fungal activity found that the surfaces of marble specimens on which bird excreta had been deposited supported the growth of several species of fungi (Bassi and Chiatante 1976). In separate experiments, two of these species - *Aspergillus repens* and *Penicillium cyclopium* - displayed notably accelerated growth in agar in the presence of pigeon droppings compared to agar alone. These two species were also found to lower the pH of the medium (Czapek solution) in which they were grown. After fungal growth, SEM examination of the marble surfaces found numerous cavities and indentations in the surface, attributed in part to production of acid.

Slight acidification has also been observed during the growth of unidentified mould on pigeon excreta (Spennemann et al. 2017). The pH dropped from a value of 6.0 down to 5.4, over a period of 3 days, but then increased over the next 8 days to a pH of 8.5. The reason for this change was not explored further, but the most likely explanation would be the further degradation of glyoxylic acid (or other organic acids), and of urea to ammonia (Bachrach 1957). Whilst complete degradation of glyoxylic acid to CO_2 by bacteria is possible (Hutchinson 1950), formation of oxalic acid is often an intermediate stage in this process, with a proportion being precipitated as oxalate salts (Carlile 1984). This would also produce an increase in pH.

Thus, the production of glyoxylic acid via fungal degradation of uric acid in bird excreta would appear to be a potential deterioration mechanism for materials on the exterior of buildings. Damage to construction materials by organic acids does not always occur solely as a result of acidolysis. Firstly, complex formation between the organic acid and metal ions from the material may exacerbate the process of acidolysis, by increasing the concentration of ions that can be accommodated in solution, potentially leading to faster rates of deterioration. Secondly, insoluble salts can be formed with metal ions in the material. In some cases, these occupy a much larger volume than the original solid compounds, leading to expansion and cracking (Larreur-Cayol et al. 2011).

Glyoxylic acid ($OCHCO_2H$) is a highly soluble acid. In solution, the glyoxylate ion undergoes hydration in the presence of water:

$$OCHCO_2^- + H_2O \rightleftharpoons (HO)_2CHCO_2^-$$

With regards to complex formation, considering the inorganic, non-metallic components encountered in the outer fabric of buildings, the most common constituent chemical elements are likely to be calcium, silicon, aluminium, magnesium and iron, plus oxygen, carbon and hydrogen. The ability of glyoxylic acid to form complexes with these elements has not been explored thoroughly. However, the stability constants of strong complexes formed by aluminium and iron (III) have been determined (Table 1). Stability constants for iron (III) complexes have also been determined by Vincze (1999). The methods used by this researcher concluded that four complexes existed (1:1 to 1:4), and attributed very different stability constants. The stability constants adopted here were favoured on the grounds that a technique for estimating stability constants based on the affinity of metal ions for the hydroxide ion (Hancock and Martell 1989) gave a value for the aluminium glyoxylate complex with a metal ligand ratio of 1:1 close to the experimentally determined value.

The formation of salts by glyoxylic acid is also an under-explored area, but work carried out in the 19th century identified two calcium salts of low solubility (Debus 1904). These were calcium glyoxylate ($Ca(C_2HO_3)_2.2H_2O$), which forms at pH conditions around neutrality, and a basic calcium glyoxylate $Ca(OH).C_2HO_3.H_2O$ which was found to form under higher pH conditions. The second of these compounds decomposed to calcium oxalate and calcium glycolate, with elevated temperatures accelerating this process. The solubility products of the two salts are given in Table 2. It should be noted that the solubility of the basic salt is estimated based on the conventional interpretation of the term 'sparingly soluble': the solubility was assumed to be 0.1 g in 100 ml. While other salts of glyoxylic acid exist, they are more soluble. Tables 1 and 2, also contain data for oxalic acid and glycolic acid, the significance of which will become clear later in this paper.

This paper examines the behaviour of stone and concrete exposed to glyoxylic acid solutions, with the view to answering the following research questions: (i) How damaging is glyoxylic acid attack, and are some materials more vulnerable than others? (ii) To what extents do acidolysis, complex formation and the precipitation of glyoxylate salts play a role in the deterioration of stone and concrete exposed to glyoxylic acid? (iii) Based on the deterioration mechanisms, what measures are best suited to limiting glyoxylic acid attack?

The approach adopted was to initially examine the influence of the acid on two types of stone (a sandstone and a limestone) and two types of hardened cement. This was done in terms of mass loss and pH measurements from specimens submerged in acid solutions, CT scans of specimens after exposure, analysis of the altered solutions, and chemical and mineralogical analysis of the deteriorated materials. Geochemical modelling was employed to further explore the mechanism of deterioration.

2. MATERIALS AND METHODS

The approach adopted in investigating the effect of glyoxylic acid on stone and cement was to expose selected materials to solutions containing glyoxylic acid at two different concentrations, and to monitor deterioration via mass loss measurements and micro-CT scanning. Since acid attack was anticipated to leave behind residual constituents of the original materials, and possibly glyoxylate salts, it was decided

that chemical and mineralogical analysis of the acid degraded layers would also shed light on the mechanisms involved. In addition, analysis of the solutions after the experiments would assist in elucidating the chemical reactions occurring.

Table 1. Stability constants of complexes formed between selected metal ions and glyoxylic, oxalic and glycolic acid.

SPECIES	REACTION	STABILITY CONSTANT, Log K	REF.
Glyoxylic Acid			
H	$H^+ + C_2HO_3^- \rightleftharpoons C_2H_2O_3$	3.46	Martell and Smith (2001)
Al			
$Al(Glyoxylate)^{2+}$	$Al^{3+} + C_2HO_3^- \rightleftharpoons Al(C_2HO_3)^{2+}$	13.5	
$Al(Glyoxylate)_2^+$	$Al^{3+} + 2C_2HO_3^- \rightleftharpoons Al(C_2HO_3)_2^+$	22.8	Smith and Doctor (1975)
Fe(III)			
$Fe(Glyoxylate)^{2+}$	$Fe^{3+} + C_2HO_3^- \rightleftharpoons Fe(C_2HO_3)^{2+}$	13.9	
$Fe(Glyoxylate)_2^+$	$Fe^{3+} + 2C_2HO_3^- \rightleftharpoons Fe(C_2HO_3)_2^+$	26.1	
Oxalic Acid			
H	$H^+ + C_2O_4^{2-} \rightleftharpoons C_2HO_4^-$	4.19	Martell and Smith (2001)
	$2H^+ + C_2O_4^{2-} \rightleftharpoons C_2H_2O_4$	5.42	
Ca			
Ca(Oxalate)	$Ca^{2+} + C_2O_4^{2-} \rightleftharpoons Ca(C_2O_4)$	3.19	
$Ca(Oxalate)_2^{2-}$	$Ca^{2+} + 2C_2O_4^{2-} \rightleftharpoons Ca(C_2O_4)_2^{2-}$	8.10	Martell and Smith (2001)
$CaH(Oxalate)^+$	$Ca^{2+} + C_2O_4^{2-} + H^+ \rightleftharpoons CaH(C_2O_4)^+$	6.03	
$CaH_2(Oxalate)_2$	$Ca^{2+} + 2C_2O_4^{2-} + 2H^+ \rightleftharpoons CaH_2(C_2O_4)_2$	10.18	
Al			
$Al(Oxalate)^+$	$Al^{3+} + C_2O_4^{2-} \rightleftharpoons Al(C_2O_4)^+$	7.7	
$Al(Oxalate)_2^-$	$Al^{3+} + 2C_2O_4^{2-} \rightleftharpoons Al(C_2O_4)_2^-$	13.4	
$Al(Oxalate)_3^{3-}$	$Al^{3+} + 3C_2O_4^{2-} \rightleftharpoons Al(C_2O_4)_3^{3-}$	17.0	
$AlH(Oxalate)^{2+}$	$Al^{3+} + C_2O_4^{2-} + H^+ \rightleftharpoons AlH(C_2O_4)^{2+}$	7.5	Martell and Smith (2001)
AlOH(Oxalate)	$Al^{3+} + C_2O_4^{2-} + H_2O \rightleftharpoons AlOH(C_2O_4) + H^+$	2.6	
$AlOH(Oxalate)_2^{2-}$	$Al^{3+} + 2C_2O_4^{2-} + H_2O \rightleftharpoons AlOH(C_2O_4)_2^{2-} + H^+$	6.8	
$Al(OH)_2(Oxalate)^-$	$Al^{3+} + C_2O_4^{2-} + 2H_2O \rightleftharpoons Al(OH)_2(C_2O_4)^- + 2H^+$	-3.1	
Fe(II)			
Fe(Oxalate)	$Fe^{2+} + C_2O_4^{2-} \rightleftharpoons Fe(C_2O_4)$	3.97	Martell and Smith (2001)
$Fe(Oxalate)_2^{2-}$	$Fe^{2+} + 2C_2O_4^{2-} \rightleftharpoons Fe(C_2O_4)^{2-}$	5.90	
Fe(III)			
$Fe(Oxalate)^+$	$Fe^{3+} + C_2O_4^{2-} \rightleftharpoons Fe(C_2O_4)^+$	9.15	Martell and Smith (2001)
$Fe(Oxalate)_2^-$	$Fe^{3+} + 2C_2O_4^{2-} \rightleftharpoons Fe(C_2O_4)_2^-$	15.45	
$Fe(Oxalate)_3^{3-}$	$Fe^{3+} + 3C_2O_4^{2-} \rightleftharpoons Fe(C_2O_4)_3^{3-}$	19.83	
$FeH(Oxalate)^{2+}$	$Fe^{3+} + C_2O_4^{2-} + H^+ \rightleftharpoons FeH(C_2O_4)^{2+}$	4.35	Christodoulou et al. (2001)
Mg			
Mg(Oxalate)	$Mg^{2+} + C_2O_4^{2-} \rightleftharpoons Mg(C_2O_4)$	2.76	Martell and Smith (2001)
$Mg(Oxalate)_2^{2-}$	$Mg^{2+} + 2C_2O_4^{2-} \rightleftharpoons Mg(C_2O_4)_2^{2-}$	4.24	
Si			
Si(Oxalate)	$H_4SiO_4 + C_2O_4^{2-} \rightleftharpoons Si(C_2O_4)(OH)_4^{2-}$	0.04	Öhman et al. (1991)
Glycolic Acid			
H	$H^+ + HOCH_2CO_2^- \rightleftharpoons HOCH_2CO_2H$	3.83	
Ca			
$Ca(Glycolate)^+$	$Ca^{2+} + HOCH_2CO_2^- \rightleftharpoons Ca(HOCH_2CO_2)^+$	1.62	
Fe (II)			
$Fe(Glycolate)^+$	$Fe^{2+} + HOCH_2CO_2^- \rightleftharpoons Fe(HOCH_2CO_2)^+$	1.33	Martell and Smith (2001)
Fe (III)			
$Fe(Glycolate)^{2+}$	$Fe^{3+} + HOCH_2CO_2^- \rightleftharpoons Fe(HOCH_2CO_2)^{2+}$	2.90	
$Fe(Glycolate)^+$	$Fe^{3+} + HOCH_2CO_2^- \rightleftharpoons Fe(OCH_2CO_2)^+ + H^+$	4.21	

$Fe(Glycolate)_2$	$Fe^{3+} + 2HOCH_2CO_2^- \rightleftharpoons Fe(CH_2OCO_2)(OCH_2CO_2) + H^+$	6.61
$Fe(Glycolate)_3^{2-}$	$Fe^{3+} + 3HOCH_2CO_2^- \rightleftharpoons Fe(CH_2OCO_2)_2(OCH_2CO_2)^{2-} + 2H^+$	8.11
Mg		
$Mg(Glycolate)^+$	$Mg^{2+} + HOCH_2CO_2^- \rightleftharpoons Ca(HOCH_2CO_2)^+$	0.92

Table 2. Solubility products of salts formed between selected metal ions and glyoxylic, oxalic and glycolic acids.

COMPOUND	FORMULA / REACTION	SOLUBILITY PRODUCT, log K_{sp}	REF.
Glyoxylic Acid			
Calcium glyoxylate	$Ca(C_2HO_3)_2.2H_2O \rightleftharpoons Ca^{2+} + 2C_2HO_3^- + 2H_2O$	-6.54	Debus (1904)
Basic calcium glyoxylate*	$Ca(OH).C_2HO_3.H_2O \rightleftharpoons Ca^{2+} + C_2HO_3^- + OH^- + H_2O$	"sparingly soluble" (-6.51)	Debus (1904)
Potassium glyoxylate	$K(C_2HO_3).H_2O \rightleftharpoons K^+ + C_2HO_3^- + H_2O$	"highly soluble"	Joint Chemical and Pharmaceutical Company (2017)
Magnesium glyoxylate	$Mg(C_2HO_3)_2 \rightleftharpoons Mg^{2+} + 2C_2HO_3^-$	2.62	Streit et al. (1998)
Oxalic Acid			
Calcium oxalate	$Ca(C_2O_4) \rightleftharpoons Ca^{2+} + C_2O_4^{2-}$	-8.56	
Calcium oxalate monohydrate (whewellite)	$Ca(C_2O_4).H_2O \rightleftharpoons Ca^{2+} + C_2O_4^{2-} + H_2O$	-8.69	
Calcium oxalate dihydrate (weddellite)	$Ca(C_2O_4).2H_2O \rightleftharpoons Ca^{2+} + C_2O_4^{2-} + 2H_2O$	-8.35	Weast et al. (1986)
Calcium oxalate trihydrate (caoxite)	$Ca(C_2O_4).3H_2O \rightleftharpoons Ca^{2+} + C_2O_4^{2-} + 3H_2O$	-8.29	
Aluminium oxalate tetrahydrate	$Al_2(C_2O_4)_3.4H_2O \rightleftharpoons 2Al^{3+} + 3C_2O_4^{2-} + 4H_2O$	-33.46	Christodoulou et al. (2001)
Iron (II) oxalate dihydrate	$Fe(C_2O_4).2H_2O \rightleftharpoons Fe^{2-} + C_2O_4^{2-} + 2H_2O$	-4.73	Tanaka et al. (2010)
Iron (III) oxalate pentahydrate	$Fe_2(C_2O_4)_3.5H_2O \rightleftharpoons 2Fe^{3+} + 3C_2O_4^{2-} + 5H_2O$	-38.52	Christodoulou et al. (2001)
Magnesium oxalate dihydrate	$Mg(C_2O_4).2H_2O \rightleftharpoons Mg^{2+} + C_2O_4^{2-}$	-5.18	Weast et al. (1986)
Glycolic Acid			
Calcium glycolate monohydrate	$Ca(CH_2(OH)CO_2)_2{\cdot}H_2O \rightleftharpoons Ca^{2+} + 2CH_2(OH)CO_2^- + H_2O$	-2.71	Adu-Wusu (2012)
Aluminium glycolate	$Al(CH_2(OH)CO_2)_3 \rightleftharpoons Al^{3+} + 3CH_2(OH)CO_2^-$	Assumed to be soluble	-
Iron (III) glycolate	$Fe(CH_2(OH)CO_2)_3 \rightleftharpoons Fe^{3+} + 3CH_2(OH)CO_2^-$	Assumed to be soluble	-

Magnesium glycolate	$Mg(CH_2(OH)CO_2)_2 \rightleftharpoons Mg^{2+} + 2CH_2(OH)CO_2^-$	-0.55	Stanga (2010)

*See Results section – compound may not exist.

A series of geochemical models were developed using the geochemical modelling computer program PHREEQC (Parkhurst and Appelo 2013) to further understand the mechanisms of deterioration. Part of the interpretation of these results was anticipated to involve an understanding of the nature of the calcium glyoxylate salts, and, specifically, the likely effects of their precipitation on the volume stability of stone and cement. This requires knowledge of the crystal structure of the compounds, of which nothing was known. For this reason, it was also decided to synthesise and then attempt to determine the structure of these compounds using powder X-ray diffraction.

2.1 Materials and Chemical Reagents

2.1.1 Stone and cement specimens

Four materials were studied. These were a limestone, a sandstone, and two hardened cement pastes prepared from Portland and calcium aluminate cements.

The sandstone was an Old Red sandstone from a disused quarry located near John O'Groats in Scotland, whilst the limestone was Skateraw limestone, again from Scotland (Ziogos et al. 2015). Specimens were prepared by coring cylinders from larger samples with a diameter of 15mm and a length of 60mm (+/-1 mm). The sandstone was known to be cemented with aluminosilicate minerals and was selected on the grounds that, whilst the sand component was likely to resist attack, the other phases might be attacked as a result of complexation of aluminium by glyoxylate ions. The limestone was one of two readily available to the study, but was selected on the grounds that it contained both calcite and dolomite, allowing the effect of glyoxylic acid on both minerals to be examined.

Two cements were used to prepare the cement pastes – a Portland cement (PC) of strength class 52.5 as defined in EN 197-1 (British Standards Institution 2011), and a calcium sulfoaluminate (CSA) belite cement. Portland cement was chosen on the basis that it remains the common cement constituent in most concrete mixes, and in the concrete of most existing structures. CSA cement was selected on the grounds that cements of this type are growing in use in many parts of the world, with one of their key features being enhanced acid-resistance.

The cement paste specimens were mixed by hand for 3 minutes with distilled water at a water / cement ratio of 0.5. The pastes were poured into polyethylene cylinders with an internal diameter of 22 mm and a height of 70 mm. The cylinders were gently vibrated to remove as many air bubbles as possible. The cylinders were sealed and stored at 25 °C for a period of 28 days prior to the beginning of acid exposure experiments. The chemical and mineralogical compositions of the materials are provided in Tables 3 and 4 respectively. It was assumed that the amorphous component of the PC cement paste was composed primarily of calcium silicate hydrate (C-S-H) phases, whilst in the CSA paste it comprised C-S-H and aluminium hydroxide phases.

2.1.2 Reagents

All of the chemicals used during the study were of a reagent grade. These were glyoxylic acid (>99% purity), 35% ammonia solution and calcium nitrate tetrahydrate (>95% purity). Chromatographic grade corundum was used as an internal standard for powder X-ray diffraction analyses.

2.2 Synthesis of Calcium Glyoxylate Compounds

To synthesise the neutral calcium glyoxylate salt, a method outlined by Debus (1904) was used as the basis. The only significant difference was that the original method utilised solid ammonium glyoxylate added to water, whereas the approach adopted for this study was to synthesise this compound *in-situ*.

Table 3. Chemical compositions of the stone and cement pastes obtained using X-ray fluorescence spectrometry.

	% by mass			
CONSTITUENT	**Limestone**	**Sandstone**	**PC**	**CSA**
CaO	36.28	0.14	63.51	40.50
SiO_2	11.98	86.70	19.73	10.56
Al_2O_3	2.20	7.06	4.58	31.33
Fe_2O_3	6.72	0.47	2.61	2.26
MgO	5.86	0.30	0.93	1.49
MnO	0.17	0.01	0.04	0.02
TiO_2	0.15	0.19	0.22	1.38
Na_2O	0.10	0.10	0.26	0.08
K_2O	0.30	2.83	0.52	0.26
P_2O_5	0.17	0.05	0.23	0.09
SO_3	1.260	0.018	3.192	7.912
Cl	0.048	nd	0.043	0.030

nd = not detected.

Table 4. Mineralogy of the stone and hydrated cement paste specimens estimated using Rietveld refinement of powder X-ray diffraction traces.

		% by mass						
PHASE		**Initial Composition**				**Acid-Degraded Layer**		
	FORMULA	**Limestone**	**Sandstone**	**PC**	**CSA**	**Limestone**	**PC**	**CSA**
Calcite	$CaCO_3$	48.4	-	2.0	0.2	-	-	-
Quartz	SiO_2	9.3	81.2	-	-	55.4	1.0	-
Dolomite	$CaMg(CO_3)_2$	42.3	-	-	-	14.3	-	-
Sanidine	$K(AlSi_3O_8)$	-	10.0	-	-	-	-	-
Muscovite	$KAl_2(AlSi_3O_{10})(OH)_2$	-	4.6	-	-	-	-	-
Kaolinite	$Al_2Si_2O_5(OH)_4$	-	4.2	-	-	10.9	-	-
C_2S	Ca_2SiO_4	-	-	3.9	3.2	-	-	-
C_3S	Ca_3SiO_5	-	-	1.9	-	-	-	-
C_3A	$Ca_3Al_2O_6$	-	-	0.2	0.7	-	-	-
C_4AF	$Ca_4Al_2Fe_2O_{10}$	-	-	0.8	-	-	-	-
Ettringite	$Ca_6Al_2(SO_4)_3(OH)_{12}\cdot 26H_2O$	-	-	2.1	4.3	-	-	-
Monosulfate	$Ca_4Al_2(SO_4)(OH)_{12}\cdot 6H_2O$	-	-	0.1	18.5	-	-	-
Hemicarbonate	$Ca_4Al_2(CO_3)_{0.5}(OH)_{13}.5.5H_2O$	-	-	0.5	-	-	-	-
Monocarbonate	$Ca_4Al_2(CO_3)(OH)_{12}\cdot 5H_2O$	-	-	1.3	-	-	-	-
Portlandite	$Ca(OH)_2$	-	-	8.9	-	-	-	-
Strätlingite	$Ca_2Al_2SiO_2(OH)_{10}\cdot 3H_2O$	-	-	-	7.6	-	-	-
Gibbsite	$Al(OH)_3$	-	-	-	1.4	-	-	37.0
Perovskite	$CaTiO_3$	-	-	-	2.4	-	-	2.5

Gehlenite	$Ca_2Al_2SiO_7$	-	-	-	3.8	-	-	-
Ye-elimite	$Ca_4(AlO_2)_6SO_4$	-	-	-	0.7	-	-	-
Hematite	Fe_2O_3					0.9	-	-
Weddellite	$CaC_2O_4{\cdot}2H_2O$					18.5	32.4	1.8
Whewellite	$CaC_2O_4{\cdot}H_2O$					-	4.4	10.5
Amorphous	-	-	-	78.3	57.1	-	62.2	48

100ml of a 1M solution of glyoxylic acid was prepared using distilled water and the pH adjusted to a value of 7.0 by the addition of 35% ammonia solution. This solution was then mixed with a 0.5M solution of calcium nitrate, yielding a white precipitate. The precipitate was initially amorphous when analysed using powder X-ray diffraction. However, after being left for a period of 48 hours, and allowing the majority of water to evaporate, crystalline material had formed on the sides of the beaker. The precipitate was washed and filtered using vacuum filtration and dried in a vacuum oven at 20 °C.

An attempt was also made to synthesise the basic salt, again following a method outlined by Debus (1904). A saturated solution of calcium hydroxide was prepared by adding an excess of freshly calcined calcium oxide to a beaker and filtering the resulting mixture using vacuum filtration. A 1M solution of glyoxylic acid was added dropwise to the lime solution followed by shaking until a permanently cloudy liquid was obtained. This was filtered and dried as before. As discussed later, the basic salt was not successfully obtained.

2.3 Mass Loss Experiments

Four 4 litre 0.10 M solutions of glyoxylic acid were prepared using distilled water in polyethylene tanks with a maximum capacity of 5 litres. pH measurements were made on the solutions prior to starting the experiments using a portable pH meter.

Each tank was used to hold one specimen. A single specimen of each material was used for each mass loss experiment, and subsequent CT scans. Stone specimens were placed into their tank in an air-dry condition, after being weighed. The cement pastes were removed from their polyethylene cylinders, weighed immediately, and placed into their tanks.

Measurements of specimen mass and solution pH were made periodically for a period of 90 days. Specimens were removed from their solutions and excess solution removed by patting dry with absorbent paper, meaning that the specimen was weighed in a saturated, but surface-dry, condition. Further drying was not attempted, on the grounds that the acid-degraded layers of cement pastes are extremely vulnerable to shrinkage and cracking when dried.

2.4 Micro-CT Scanning

After removal of the specimens from their tanks, they were immediately dried in a vacuum chamber at 20 °C. Micro-CT scans of the specimens were obtained using a Nikon XTH225ST scanner. The specimens were located 150 mm away from the X-ray source, with a 0.5 mm copper filter to obtain a suitable image quality. A tungsten excitation target lens under operating conditions of 115 kV and 312 µA was employed. Under these conditions the resolution of the image was such that 1 pixel width was equivalent to 14.97 µm. The specimens were revolved in increments of 0.11 ° and images were generated using a 2-frame averaging technique at each increment.

Measurement of the dimensions of the acid-degraded layers of the materials employed image analysis techniques using the scanner's software to fit cylinder shapes to the 3-dimensional images of these layers, thus obtaining a single average value for each dimension.

2.5 Analysis of Degraded Layers after Acid Exposure

2.5.1 Powder X-ray diffraction (XRD)

Where the outer layers of the specimens were altered by exposure to the acid solutions, this layer was removed after CT scanning using a scalpel and analysed using a Siemens D5000 powder X-ray diffractometer using a Cu-kα source operating at 40 mA and 40 kV. Scans were obtained using angular increments of 0.10 °2θ at a rate of 0.67 °2θ minute^{-1}. Two sub-samples per specimen were prepared and analysed – one in an unadulterated form, and one to which a 5% by mass corundum internal standard was added and mixed.

The X-ray diffraction traces obtained from the samples containing internal standards were analysed by Rietveld refinement, again using the MAUD program. During refinement, iron was permitted to substitute for aluminium in the monosulfate and AFt cement hydrate phases, where present. Rietveld refinement allowed the crystalline constituents of the material to be estimated. Additionally, since the quantity of corundum present was known, this allowed the amorphous content of the material to be estimated and the quantities of crystalline phases to be scaled accordingly.

Sediment which accumulated on the bottom of the tanks was also collected, filtered, vacuum dried and analysed using X-ray powder diffraction. These samples were of insufficient quantity to allow the introduction of an internal standard and analysis using Rietveld refinement.

2.5.2 X-ray fluorescence spectrometry

The subsample of the degraded layer material which was unadulterated with internal standard was then pressed into pellets for elemental analysis using a using a Panalytical Zetium 2.4W X-ray fluorescence spectrometer. Analysis was conducted using a RhKα source under vacuum conditions. The analytical procedure utilised LiF200, Ge111, PE002, PX-1 and LiF220 diffraction crystals, and used MCA flow, sealed Xe and MCA scintillation detectors.

2.6 Analysis of the Acid Solutions

The acid solutions in each tank were analysed using UV/VIS spectrometry at the end of the experiment to establish changes in composition in terms of organic species and / or complexes formed between ions deriving from the specimens. A Jenway 7315 UV/VIS spectrometer was used with 2.5ml UV cuvettes. Scans across a wavelength range of 200-1000 nm were run, in increments of 1 nm. Solutions from the tanks were pipetted into a cuvette and diluted with distilled water such that any absorbance peaks fell within the maximum absorbance range of the instrument.

2.7 Geochemical Modelling

Geochemical modelling was conducted using the PHREEQC computer program (Parkhurst and Appelo 2013). The approach adopted was to model the diffusion of acidic species through the porosity of the specimens, and predict their interaction with the solid constituents.

The model consisted of a series of cells linked in sequence. In the case of the cement specimens, 102 cells were used, whereas 77 cells were used for the stone models to reflect the difference in radius of the two types of specimen. The first cell contained a mass of 4 kg of water in which 0.4 moles of glyoxylate ion was dissolved, representing the exposure tank. The second cell contained 467 mg of water with the same concentration of glyoxylic acid, and was used to account for the possibility that salts might be precipitated against the specimen surface. These two cells were followed by the remaining cells, which were 0.1 mm long and contained a quantity of pure water and a mineral assemblage which reflected the composition of the specimen being modelled, and thus represented the stone and cement specimens and their pore solutions. In the case of the stone specimens the cells contained 233 mg of water, whilst the cells of the cement specimens contained 438 mg. These values were chosen to

represent a total porosity of around 16% for all specimens. Successive layers beneath the surface of a cylindrical specimen clearly decline in volume, whilst in the model this volume remained uniform. Since a proportion of each specimen remained unaltered by exposure at the end of the experiments, this deviation from the actual conditions was unlikely to compromise the model's ability to reflect the experimental conditions.

In the case of the stone specimens, the mineral assemblage composition was based on the Rietveld refinement results. In the case of the sandstone model, each cell initially contained a total 0.28 g of solid material, to give a total mass of material equal to the sandstone specimen mass. In the case of limestone, the assemblage mass per cell was 0.23 (specimen mass = 22.80 g).

In the case of the cement paste specimens, the mineral assemblage was derived from an optimisation process which arrived at an assemblage of cement hydration products which satisfied the chemical compositions in Table 3 (in terms of CaO, SiO_2, Al_2O_3, Fe_2O_3 and SO_3). During optimisation, the molar Ca/Si ratio of the calcium silicate hydrate phase was allowed to change between 0.7 and 2.3, which is the typical compositional range of this substance. Additionally, due to the insolubility of perovskite, the composition of the CSA cement mineral assemblage was modified to discount this phase. The mass of mineral assemblage in each cement specimen cell was 0.42 g for PC (actual specimen mass = 42.93 g) and 0.40 g for CSA (actual specimen mass = 42.57 g).

The mineral assemblages included under the PHREEQC 'EQUILBRIUM_PHASES' keyword in the models devised for each specimen are shown in Table 5.

The basic dataset used for PHREEQC speciation calculations was the MINTEQ database (U.S. Environmental Protection Agency 1999). This was augmented with cement hydrate data collated by Lothenbach et al. (2008), plus the values in Tables 1 and 2. To take into account the variability in composition of the C-S-H phase, the approach adopted by De Windt and Devillers (2010) using existing solubility data (Stronach and Glasser 1997) was employed: C-S-H phases with molar Ca/Si ratios of 0.8, 1.1 and 1.8 were included in the database, along with the MINTEQ database mineral 'amorphous silica gel' (log K_{sp} = 2.71).

The MINTEQ database did not contain solubility data for muscovite or sanidine. Therefore the following dissolution reactions and solubility products were added:

muscovite:

$$KAl_2(AlSi_3O_{10})(OH)_2 + 12H_2O \rightleftharpoons K^+ + 3Al(OH)_4^- + 3H_4SiO_4 + 2H^+ \quad \text{Log } K_{sp} = -44.64$$

(Arnórsson and Stefánsson 1999)

sanidine:

$$KAlSi_3O_8 + 8H_2O \rightleftharpoons K^+ + Al(OH)_4^- + 3H_4SiO_4 \quad \text{Log } K_{sp} = -22.34$$

(Reesman and Keller 1965)

To allow the precipitation of phases not originally present in the mineral assemblages during exposure to the acid solution, additional phases were included in the PHREEQC 'EQUILIBRIUM_PHASES' list of the pore cells in quantities of zero moles. These phases are marked with a '0' in Table 5. In addition, all phases included in this list were included in the external solution 'EQUILIBRIUM_PHASES' list, with all quantities set to zero, to permit precipitation in the exposure tank or at the specimen surface.

The acid solution was given a pE value of 8.45, which is appropriate for water containing dissolved oxygen (Chapman 1996). This redox potential was also adopted for the interior of the stone pore solutions. The redox potential of the cement pore solutions was set to a pE of 2.54. This is typical of cement where sulfides are absent, which is the case for the materials used (Glasser 1992).

Mass transport through the specimens was modelled using the PHREEQC TRANSPORT keyword with diffusion as the sole process. Boundary conditions were set such that the first (exposure tank) and last (innermost cell of the specimen) were both closed. Each cell was 0.1 mm long.

Table 5. Mineral assemblages used for the geochemical modelling of glyoxylic acid attack.

CONSTITUENT	MATERIAL			
	Limestone	Sandstone	PC	CSA
Calcite	1.01×10^{-3}	-	-	-
Quartz	3.23×10^{-4}	3.45×10^{-3}	-	-
Dolomite	4.80×10^{-4}	-	-	-
Sanidine	-	9.18×10^{-5}	-	-
Muscovite	-	2.93×10^{-5}	-	-
Kaolinite	-	4.17×10^{-5}	-	-
Portlandite	-	-	3.28×10^{-3}	0
CSH (Ca/Si = 0.8)	-	-	5.94×10^{-4}	2.75×10^{-4}
CSH (Ca/Si = 1.1)	-	-	0	0
CSH (Ca/Si = 1.8)	-	-	0	0
Monosulfate	-	-	1.24×10^{-4}	3.68×10^{-4}
Monosulfate (iron)	-	-	6.14×10^{-5}	2.93×10^{-5}
C_2AH_8	-	-	5.99×10^{-5}	3.71×10^{-4}
C_2FH_8	-	-	1.44×10^{-5}	2.74×10^{-5}
C_3AH_6	-	-	0	0
Gibbsite	-	-	0	9.44×10^{-4}
Ferrihydrite	-	-	0	0
Calcium glyoxylate	0	-	0	0
Calcium oxalate monohydrate	0	-	0	0
Aluminium oxalate tetrahydrate	0	-	0	0
Iron (II) oxalate dihydrate	0	-	0	0
Iron (III) oxalate pentahydrate	0	-	0	0
Magnesium oxalate dihydrate	0	-	0	0
Calcium glycolate monohydrate	0	-	0	0
CO_2 (gas)	0	-	-	-

The geochemical models were adjusted to reflect reality by modifying the diffusion coefficient such that the final pH of the modelled exposure solution matched the experimental value within 0.1 of a pH unit. The model did not account for changes in porosity resulting from dissolution of material or precipitation of solids. Therefore, the diffusion coefficients arrived at were very much *effective* rather than absolute values. Based on the results of the experiments, additional features were also added to the models. These are detailed later in the discussion of the results of modelling.

3. RESULTS

3.1 Synthesis of Calcium Glyoxylate Compounds

3.1.1 Basic calcium glyoxylate

Whilst calcium glyoxylate was successfully synthesised, attempts to obtain the basic salt yielded only a mixture of the weddellite and whewellite forms of calcium oxalate. Repeated attempts to synthesise

the basic salt under different environmental conditions and reaction times failed to yield different reaction products. It is notable that a mixture of 20% weddellite and 80% whewellite yields a chemical composition which is very close to that proposed for the basic salt. Given that this salt has only been observed in research conducted in the 19th and early 20th century, and taking into account the limited palette of analytical techniques available to researchers at that time, it is tentatively concluded that basic calcium glyoxylate is, in fact, a mixture of calcium oxalate salts.

3.1.2 Calcium glyoxylate dihydrate

Calcium glyoxylate dihydrate was successfully obtained and the structure determined and refined using a combination of simulated annealing and Rietveld refinement techniques after powder X-ray diffraction analysis. As will become evident from later results, the structure is of limited relevance in the context of this paper, and so details will be published in a separate paper. However, in summary, the compound has a tetragonal cell (dimensions: a = 9.009 Å, b = 9.034 Å, c = 10.287 Å) containing 4 stoichiometric units and a density of 1.761 g cm^{-3}.

3.2 Mass Change

Figure 1 shows the results of mass measurements on the specimens during their period of exposure to glyoxylic acid solutions. The greatest rate of mass loss was observed in the case of the limestone specimen, which underwent a process of disintegration, whereby relatively large particles broke away from the specimen and fell to the bottom of the exposure tank. Exposure was stopped at 60 days for this specimen, since further disintegration might have made it difficult to image using the CT-scanner.

Both cement paste specimens lost considerable quantities of mass during exposure. Initially, the rate was highest for PC, but mass loss from the CSA specimen persisted, leading to its losing twice as much mass by 90 days. No mass loss was observed from the sandstone specimen. Indeed, there was a small gain in mass, presumably as a result of absorption of the acid solution into the specimen's porosity.

Also shown in Figure 1 are the pH measurements made on the exposure solution. In the case of the two cement pastes and limestone there is a slight increase in pH. This behaviour has not been observed in the case of similar monoprotic organic acids present at the same concentration in contact with cement paste specimens (Dyer 2017), since the materials typically do not have the capacity to wholly neutralise the acid. These results strongly suggest the precipitation of acid species from solution in the exposure tank. Indeed, sediment at the bottom of the tanks containing the limestone and cement paste specimens was evident. In the case of the limestone and CSA specimens, this appeared - at least in part – to be material falling away from the specimens. However, in the case of the PC specimen, this appeared to be solely a precipitate from solution.

It was also noted that the solutions in contact with the limestone, PC and CSA specimens started to develop a faint greenish-yellow colour.

3.3 Micro-CT Scans

Figure 2 shows sections through the specimens after exposure to glyoxylic acid. In the case of the limestone specimen exposure caused significant damage, with substantial loss of material as a result of disintegration. Volume analysis of the 3-dimensional image obtained from CT scanning indicated a loss of volume of 47%, which fits well with the loss of mass measured. This approximates to an average loss of material to a depth of 2.05 mm, although this loss is, in reality, uneven.

The scan image features an interesting feature – an acid deteriorated layer which appears only in parts of the specimen. This layer appears to be housed within a thin 'skin' of material which follows the shape

of the original specimen, but beneath this is a high porosity layer composed of discrete particles. In contrast, the sandstone specimen appeared wholly unaffected by contact with glyoxylic acid.

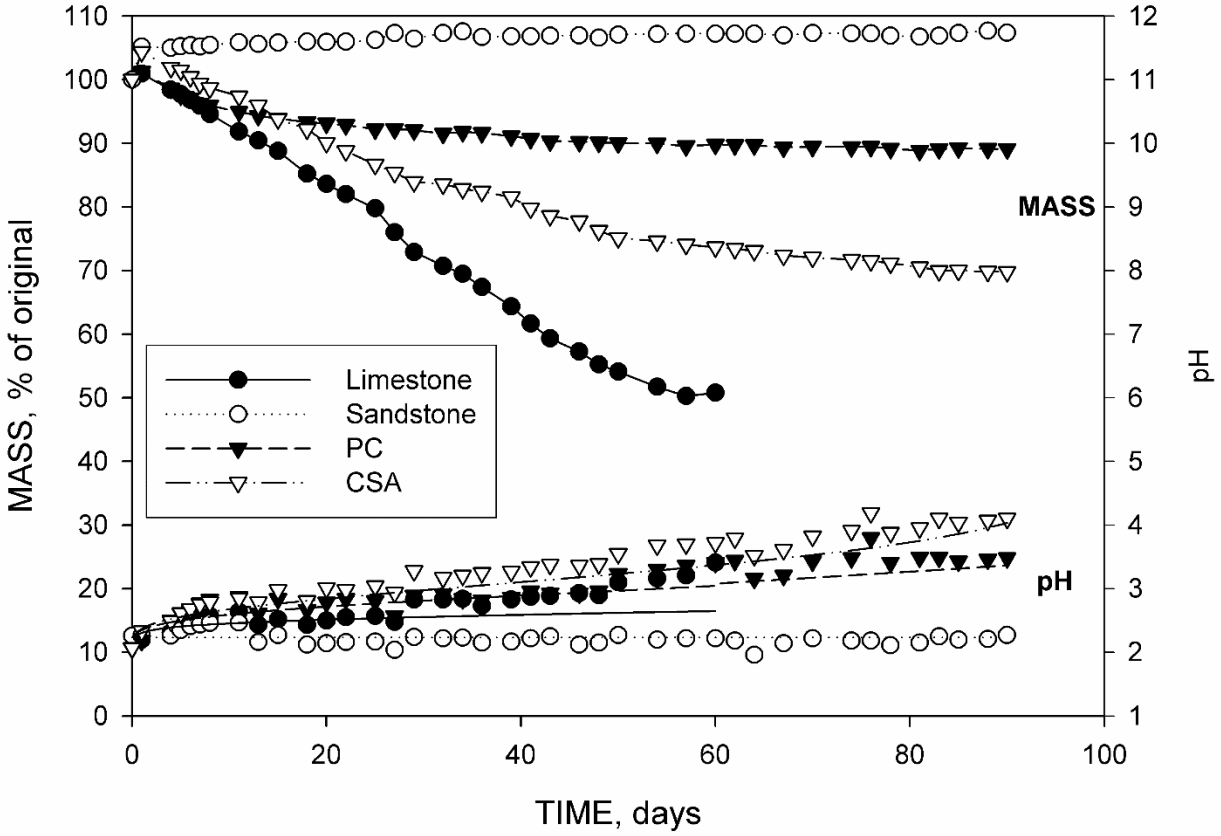

Figure 1. Mass and pH measurements from the specimens exposed to glyoxylic acid solutions. Curves for the pH plots are those obtained from geochemical modelling.

The cement paste specimens both display a common feature – a degraded layer around the outside of the specimens. In the case of Portland cement, exposure to acid initially solubilises portlandite ($Ca(OH)_2$) crystals, leading to an increase in porosity and a loss of calcium (Carde and François 1997). This process of decalcification then progresses further as calcium aluminate hydrate phases decompose and calcium is leached from the CSH phases, ultimately leaving only silica gel and some amorphous aluminium and iron hydroxide. The effects of this process are seen in Figure 2: the outside of the specimen consists of a darker silica gel layer, followed by an intermediate zone where portlandite is absent, with an unaffected core at the centre.

The section through the CSA paste shows the formation of a similar outer degraded layer. Portlandite is typically absent from hardened CSA cements, and so an intermediate zone is not present. From Figure 2 it is clear that some of the acid-degraded layer has fallen away from the CSA paste specimen. This is presumably the reason for the greater mass loss from the CSA paste, since the degraded depths observed are similar – 2.70 and 2.57 mm for PC and CSA respectively. In the case of the cement paste specimens - and from a purely structural perspective - retention of the unaffected core is proposed as being the primary measure of acid resistance, since even partial decalcification leads to a significant loss in strength (Carde and François 1997). Using this criteria, the CSA cement paste is fractionally superior at resisting glyoxylic acid attack in comparison to the PC paste.

The stone specimens had different dimensions compared to the cement paste specimens. Thus, the best means of comparing performance is in terms of the degraded volume produced in each case – i.e. the volume of material either entirely lost or altered by contact with acid. Whilst the limestone specimen disintegrated unevenly, its loss of volume is equivalent to a degraded volume of 5004 mm^3.

The calculated degraded volumes based on the degraded depths of the cement specimens were 11830 and 11350 mm^3 for PC and CSA cement paste respectively.

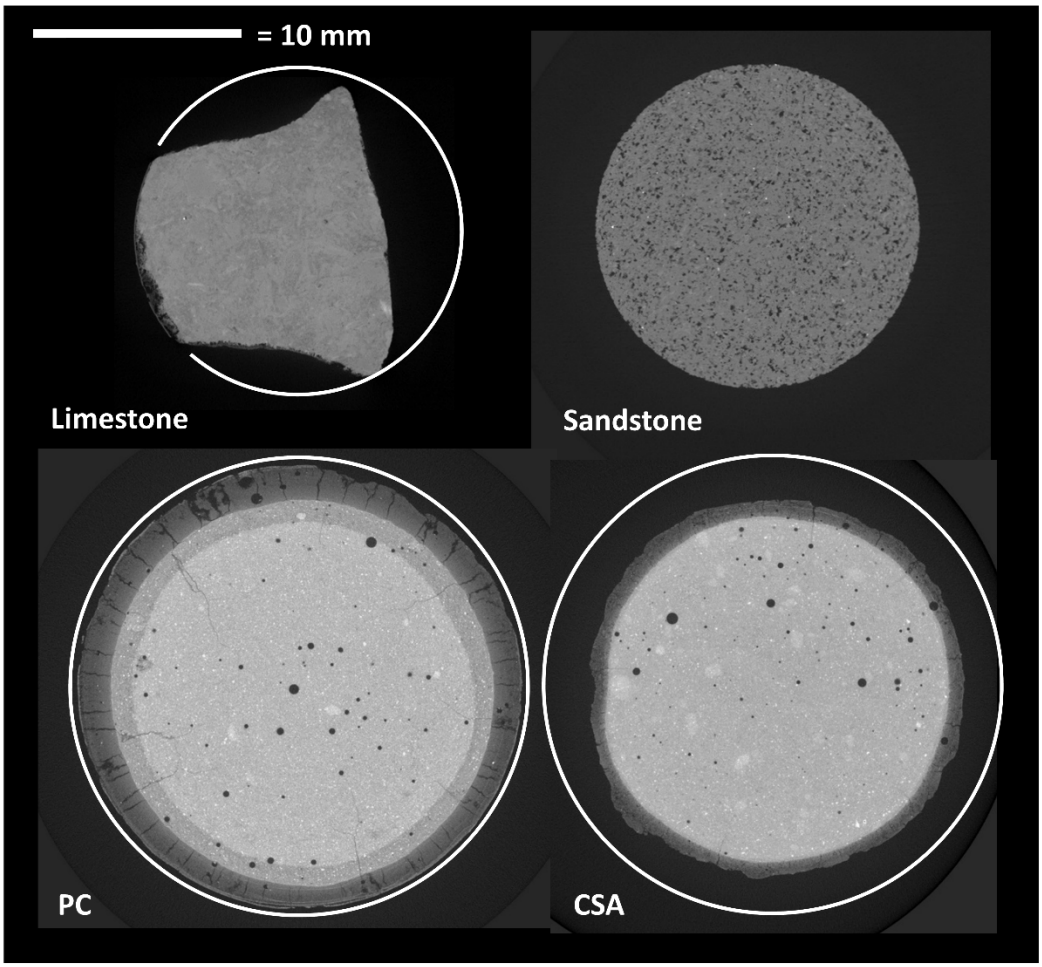

Figure 2. CT scans of the specimens after 90 days exposure to 0.1M glyoxylic acid solutions (60 days in the case of the limestone specimen). The superimposed circles represent the original cross-sectional area of the specimens.

3.4 Compositions of the Acid-Degraded Layers

The acid-degraded layers of the cement paste samples were of a relatively large volume, and so adequate quantities were available for the preparation of pellets for XRF analysis. Whilst the limestone specimen did have an acid-degraded layer, it was present in quantities insufficiently large to produce XRF pellets. However, enough was present to permit powder XRD analysis.

Table 6 shows the chemical composition of the acid-degraded layers from the cement paste specimens. For both materials there is a significant drop in CaO and SO_3 content, and a rise in SiO_2 compared to the original compositions in Table 3. The values in these two tables differ in that the latter relates to the anhydrous material and the former corresponds to material in a hydrated condition. For this reason, concentrations are also given in Table 6 normalised to 100% before and after exposure to the acid solution. When presented in this manner, differences are also evident in terms of how Al_2O_3 and Fe_2O_3 change after acid exposure. In the case of the PC specimen, both Al_2O_3 and Fe_2O_3 drop after exposure to glyoxylic acid. In contrast, the quantities of both oxides increase in the CSA specimen.

Table 6. Chemical compositions of the acid-degraded layer around the cement specimens. Also included are normalised compositions of the initial anhydrous cements compared to the acid-degraded layers, with shading indicating an increase in concentration relative to the initial value.

	% by mass		Normalised			
			PC		CSA	
CONSTITUENT	PC	CSA	Initial	Final	Initial	Final
CaO	29.56	12.71	66.25	40.54	42.23	17.35
SiO_2	38.90	17.77	20.58	53.35	11.01	24.26
Al_2O_3	2.19	35.35	4.78	3.00	32.67	48.27
Fe_2O_3	1.00	3.02	2.72	1.37	2.36	4.12
MgO	0.26	0.75	0.97	0.36	1.55	1.02
MnO	nd	0.02	0.04	nd	0.02	0.03
TiO_2	0.06	2.64	0.23	0.08	1.44	3.60
Na_2O	0.04	0.03	0.27	0.05	0.08	0.04
K_2O	0.14	0.07	0.54	0.19	0.27	0.10
P_2O_5	0.29	0.57	0.24	0.40	0.09	0.78
SO_3	0.291	0.287	3.330	0.399	8.249	0.392
Cl	0.183	0.020	0.045	0.251	0.031	0.027

nd = not detected.

Figure 3 shows the powder XRD traces obtained from the acid-degraded layers of the limestone, PC and CSA specimens, whilst the proportions of phases estimated using Rietveld refinement are in Table 4. The results are notable in that, whilst there are salts deriving from contact with glyoxylic acid, none of them are glyoxylate salts. Instead, calcium oxalate compounds have formed. These are weddellite ($CaC_2O_4 \cdot 2H_2O$) and whewellite ($CaC_2O_4 \cdot H_2O$). In the case of the PC and limestone specimens, weddellite is present to the largest extent, whilst whewellite is mainly present in the CSA layer.

It is probable that this conversion of glyoxylate to oxalate is induced by characteristics common to both the limestone and cement specimens. These are most likely the presence of dissolved calcium ions in sufficient concentrations and/or a higher solution pH.

The crystal form that calcium oxalate adopts is influenced by a number of factors including the ratio of calcium to oxalate ions and pH. Normally weddellite will form initially, later converting to whewellite if conditions are correct. Weddellite remains stable when the calcium : oxalate ratio is high (Giordani et al. 2003) and when pH is high (Manissorn et al. 2017). Neither of these factors would appear to be the sole influence in this case: the pH of both the PC and CSA pastes would be likely to lead to the dominance of weddellite, whilst the availability of calcium is presumably at an approximately comparable level for both CSA and limestone. It has also been observed that high magnesium concentrations prevent conversion (Berg et al. 1976). This potentially explains the results observed: the relatively low concentration of calcium in the CSA and limestone specimens only causes a conversion to whewellite in the case of CSA, where magnesium concentration is low. Presumably the high calcium concentrations associated with the PC specimen are sufficient to prevent conversion.

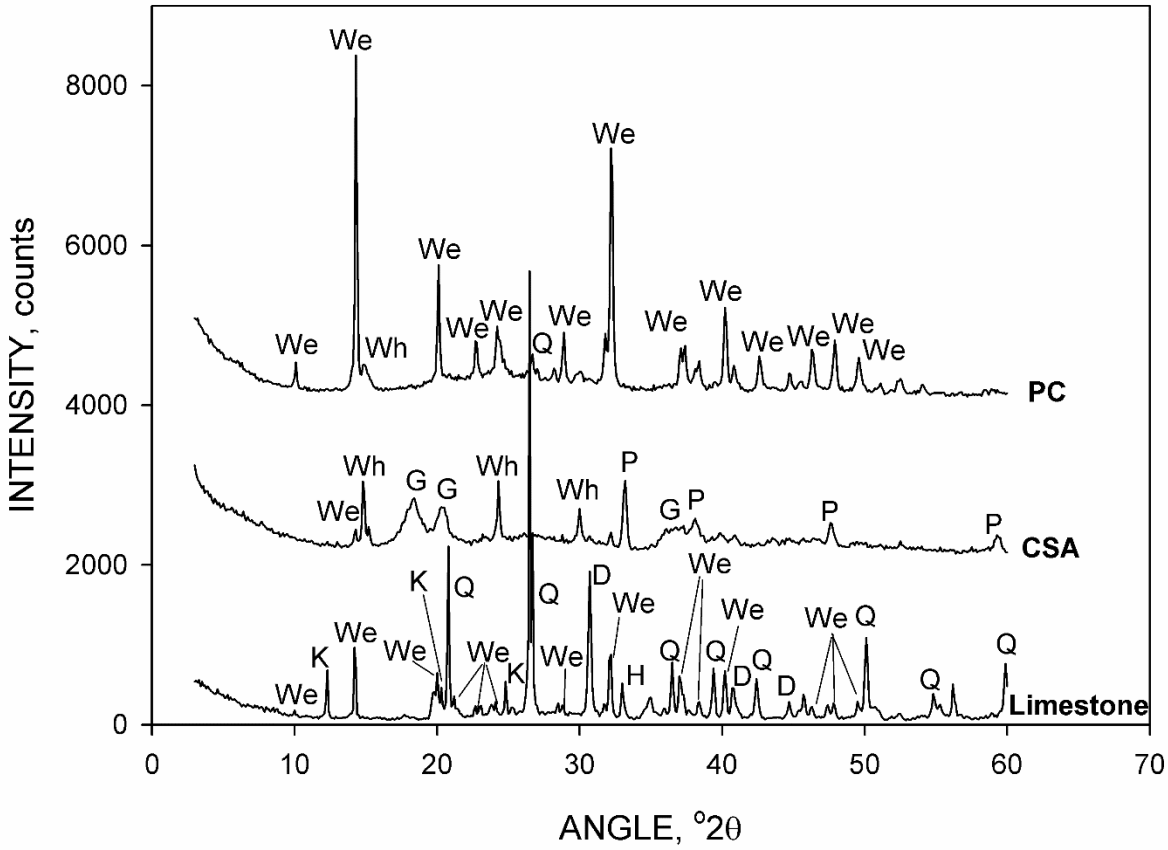

Figure 3. Powder X-ray diffraction traces from the acid-degraded layers of the limestone, PC and CSA specimens after exposure to a 0.1M glyoxylic acid solution. We = weddellite; Wh = whewellite; Q = quartz; G = gibbsite; P = perovskite; K = kaolinite; D = dolomite.

Few other phases are observed in the acid-degraded layer of the PC specimen: there is a small quantity of quartz and a substantial quantity of amorphous material, which is presumably mainly silica gel. In the case of CSA, there is also amorphous material, a quantity of poorly-crystalline gibbsite, and perovskite, which persists due to its low solubility. The acid-degraded layer of the limestone specimen contained no calcite and only a small amount of dolomite. Thus, the remaining phases in the layer were minerals of low solubility that had been present in the original material – quartz, kaolinite and hematite. Some of these constituents were originally present at such low concentrations that they were not identified during material characterisation.

Powder XRD was also conducted on sediments from the exposure tanks containing the limestone, PC and CSA specimens. The limestone sediment was of similar composition to the acid-degraded material in Figure 3, except that continued exposure of the limestone fragments had led to the complete dissolution of all carbonate minerals. The CSA sediment was again similar to the acid-degraded layer, although there appeared to be less whewellite. The sediment taken from the tank containing the PC specimen contained only weddellite. The amorphous silica gel in the acid-degraded layer (indicated by a broad hump peaking at around 25 °2θ) was entirely absent in the sediment, reinforcing the likelihood that it resulted from the precipitation of calcium oxalate from solution.

3.5 UV/VIS Spectrometry

Figure 4 shows the UV/Vis spectra obtained from the solutions at the end of the experimental period, plus a spectrum obtained from dilute glyoxylic acid. The glyoxylic acid spectrum comprises a single peak at around 225 nm. After the experiment, this peak was still present, but in the case of the limestone, PC

and CSA solutions, a broad shoulder was present on the higher wavelength side. There was a very small peak at around 310 nm in the case of the sandstone solution.

The shoulder was assumed to be composed of multiple peaks and so deconvolution was conducted using the Fityk computer program (Wojdyr 2010). Gaussian distributions were used, with three peaks yielding an adequate fit. An example of a deconvoluted spectrum is shown in Figure 4 for the PC solution.

An investigation of complexes formed between iron and glyoxylate ions employed UV spectrometer measurements at a wavelength of 254 nm (Vincze 1999). Whether this is the location of the actual peak produced by these complexes is not clear from the reference, but it is proposed that the peak at 243 nm corresponds to Fe-glyoxylate complexes, and possibly those of Al-glyoxylate.

Glyoxal ($C_2O_2H_2$) in aqueous solution produces a relatively broad peak at around 270 nm (Malik and Joens 2000), and it is proposed that the peak observed at 273 nm is this compound, meaning that the conversion reaction of glyoxylate to oxalate is likely to be:

$$2C_2HO_3^- \rightarrow C_2O_4^{2-} + C_2O_2H_2$$

This peak is responsible for the change in colour of the exposure solutions, since it encroaches into the violet region of the visible spectrum (380 - 450 nm), thus giving the solution a green-yellow colour.

The peak at 226 nm certainly includes the remaining glyoxylic acid, but peaks around this wavelength are observed for many species: for instance, it is likely that there is also a contribution from dissolved sulfate ions from the cement paste specimens.

Within the range scanned, the spectrum of oxalic acid resembles a slope running from the lowest wavelength down to around 290 nm. It is likely that this feature is present in the limestone and cement solutions, but the contribution is likely to be small as a result of the low solubility of calcium oxalate.

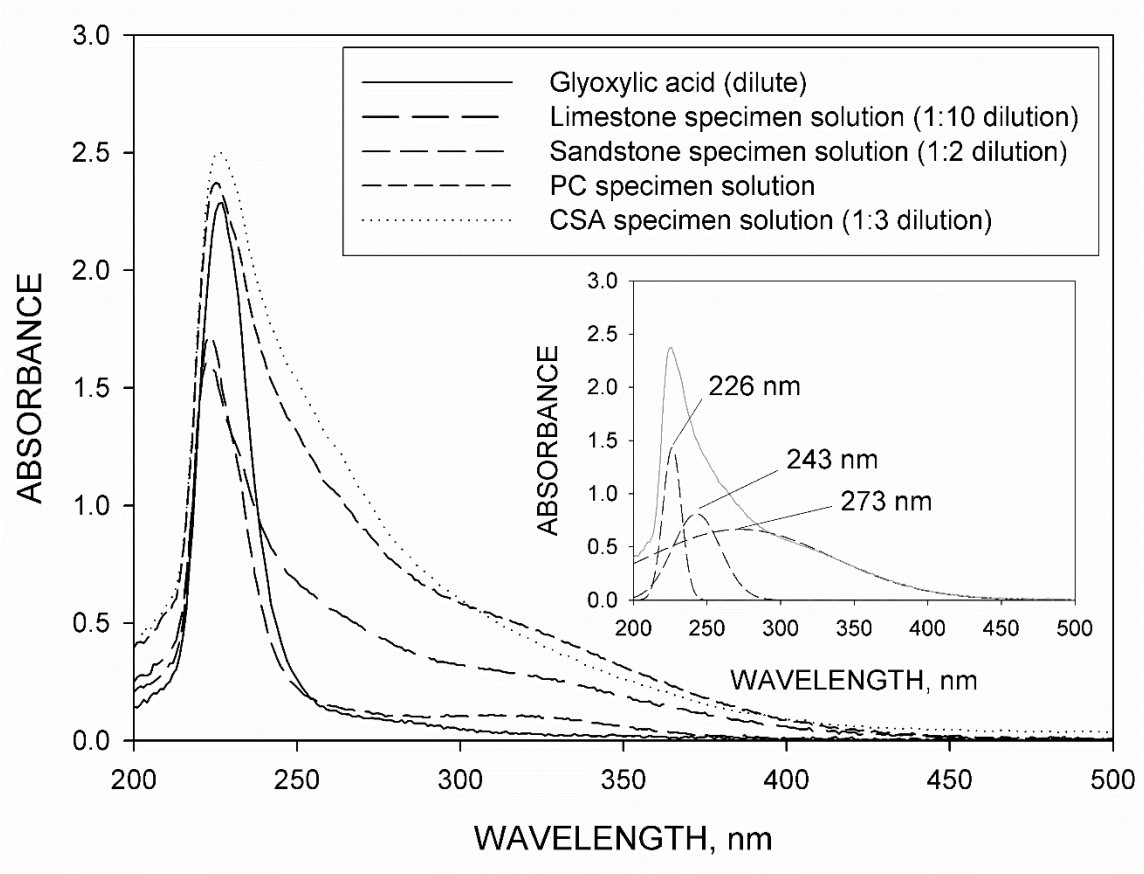

Figure 4. UV/Vis spectra from the glyoxylic acid solutions after the experiments. Inset: deconvoluted spectrum from the solution exposed to the PC specimen.

519 **3.6 Geochemical Modelling**

520 Due to conversion of glyoxylate to oxalate observed during the experiments, the geochemical models
521 were further modified to include this. It was noted that there was no evidence that calcium glyoxylate
522 was actually precipitated during the experiments. However, the conversion process was assumed for
523 modelling purposes to involve the precipitation of calcium glyoxylate followed by conversion of two
524 moles of this compound to one mole of calcium oxalate, glyoxal and calcium ions. This was done through
525 the RATES and KINETICS keywords in PHREEQC, which were used to define this chemical reaction. Since
526 little was known about the kinetics of the conversion reaction, other than its relative rapidity, the rate
527 of the reaction was set such that it was essentially instantaneous.

528 No provision was included for the transformation of weddellite to whewellite, since the nature of the
529 parameters influencing this reaction are incompletely understood, and the conversion would have
530 minimal influence on the behaviour of the models.

531 The formation of glyoxal has the potential to influence the solution chemistry of the systems being
532 modelled. Firstly, under basic conditions, glyoxal undergoes dissociation to the glycolate ion:

533 $$O{=}CHCH{=}O + OH^- \rightarrow HO\text{-}CH_2COO^-$$

534 with an acid dissociation constant of $pK_a = 3.82$ (Fratzke and Reilly 1986).

535 Furthermore, glyoxal undergoes hydration in dilute aqueous solution to form the glyoxal monomer
536 monohydrate ($O{=}CHCH(OH)_2$) and glyoxal monomer dihydrate ($[CH(OH)_2]_2$) (Schweitzer et al. 1998).
537 The dihydrate is the dominant form in solution (Fratzke and Reilly 1986). Only a hydration constant (k_H)
538 for the full hydration process from glyoxal to the monomer dihydrate has been determined ($\log k_H =$
539 4.86) (Montoya and Mellado 1995). Moreover, no acid dissociation constants are available for the
540 monomer dihydrate, but values were estimated using the ACD/I-Lab online tool. These were 11.7 and
541 13.7. This process of hydration and dissociation was incorporated into the PHREEQC models, with an
542 assumption that only the dihydrate was formed. Complex formation by the dissociated hydrate is likely
543 – it has certainly been demonstrated for copper ions (Okochi and Brimblecombe 2002). However, no
544 data exists for any of the elements included in the model, and so this aspect was also omitted.

545 Initial attempts at modelling were not able to fully replicate the increase in pH shown in Figure 1. As
546 discussed previously, precipitation of calcium oxalate is a likely cause of this rise. It was therefore
547 presumed that another mechanism was leading to further precipitation of oxalate. Since the increase
548 was only observed in the case of cement and limestone specimens, it was concluded that the additional
549 precipitation of calcium oxalate was related to the presence of glyoxal. Further investigation of the
550 chemistry of this compound revealed its ability to undergo photooxidation to form oxalic acid (Carlton
551 et al. 2007). During the experiments, the solutions would have encountered sunlight, although the
552 laboratory was glazed with conventional window glass, meaning that UV exposure was limited to
553 wavelengths above around 300 nm.

554 The photooxidation reaction also requires the presence of free radicals, which were generated in the
555 photooxidation experiments reported in the literature through the presence of hydrogen peroxide
556 (Carlton et al. 2007). Whilst this compound was not present, a potentially abundant source of radicals
557 was available in the form of oxalate ions. Oxalate radicals ($^-OOCCOO^\bullet$) are formed from oxalate ions in
558 the presence of a metal oxide catalyst (Forouzan et al. 1996). Whilst the catalyst used in the reference
559 was TiO_2, other metals could also play a similar role. Indeed, the Fenton reaction (which forms radicals
560 from hydrogen peroxide) is catalysed by aqueous iron complexes. More significantly, these can include
561 those formed with oxalate ions (Zepp et al. 1992). It is also notable that the Fenton reaction does not
562 require UV radiation, although light (<580 nm wavelength) is required to regenerate the catalyst.

563 It was therefore decided to include an oxidation reaction – potentially photocatalytic in nature - in the
564 model:

565 $$[CH(OH)_2]_2 + 2^-OOCCOO^\bullet \rightarrow 3C_2H_2O_4$$

It was assumed that concentration of oxalate radicals was directly proportional to the concentration of oxalate ions in solution. Therefore, a rate coefficient (*ak*) was used which was, in fact, the rate coefficient (*k*) multiplied by a factor (*a*) reflecting the proportion of oxalate ions that had reacted to form radicals. The reaction was assumed to be first order with respect to both glyoxal and oxalate radicals. Different combinations of diffusion and rate coefficients were explored until an appropriate pH was obtained at the end of the model run. The value of *ak* was 2×10^{-10}. Given the speculative nature of the reaction, and the use of the factor, this value should only be viewed as a means of achieving the pH levels observed in the experiments.

The diffusion coefficients which yielded fits to the experimental data were 1.00×10^{-15}, 9.00×10^{-13} and 1.02×10^{-12} $m^2\ s^{-1}$ for sandstone, PC and CSA respectively. It should be noted that whilst an adequate fit could be obtained for limestone, it required the complete dissolution of calcite, which was not observed in reality. Therefore, a diffusion coefficient of 9.00×10^{-13} $m^2\ s^{-1}$ was employed. In the case of the cement specimens, the depth of the acid degraded layer in the modelled specimens was greater than observed in the experiments. It can be concluded from these observations that additional processes involving the removal of acid species from solution were occurring.

Figure 5 shows the results of geochemical modelling of the attack of the limestone specimen by glyoxylic acid, in the form of a plot showing quantities of mineral phases present versus depth. Also shown in the figure are the dissolved concentrations of selected ions in the pore fluids of the specimen.

The outer surface is a zone containing only quartz and calcium oxalate, whilst further beneath the surface there is a second layer of acid-degraded material in which calcite has been dissolved, but dolomite remains. This reflects the lower solubility of dolomite. At the point where these two zones meet, there is an abrupt increase in pH towards the interior of the specimen. A feature of note in the dissolved species plot is a lower concentration of calcium in the acid-degraded zone where the only calcium-bearing minerals are highly insoluble oxalates.

Given that quartz is likely to been present as crystals embedded in a matrix of carbonate minerals, and the oxalate crystals will have been precipitated onto these, it is probable that the acid-degraded layer would be extremely weak. The fragments found at the bottom of the exposure tanks had essentially the same composition, and so it is proposed that once all of the dolomite is dissolved, the remaining material falls away. The second degraded layer has a composition similar to the acid-degraded material removed from the limestone specimen after exposure.

The results obtained for the modelling of acid attack of the sandstone are not shown, due to the lack of any significant change in composition. Quartz was wholly unaffected by the acid. Under the geochemical modelling regime, the other minor mineral phases did undergo alteration, with muscovite, kaolinite and sanidine dissolving and being re-precipitated as quartz. The weathering of sandstone is known to involve these processes, albeit over much longer timescales than that of the experiments. Thus, it is highly improbable that this had occurred during the experiments.

Figure 6 shows the geochemical modelling results obtained for the PC specimen. The mineral profile through the specimen closely resembles the experimental results, with an outer layer containing calcium oxalate and silica gel, followed by a partly decalcified layer where portlandite is absent and C-S-H gel with lower Ca/Si ratios is present. Beyond this layer is unaffected hydrated cement paste.

Between the outer and partly decalcified layers is a band of ferrihydrite ($Fe(OH)_3$) and gibbsite, which are typically precipitated as amorphous materials in hydrated Portland cement. The presence of such a band is commonly observed in cement and concrete attacked by acids, and manifests itself as a thin reddish-brown zone on the inside of the silica gel layer. However, the band in this instance is extremely narrow. The reason for this can be seen from the high concentration of dissolved aluminium and iron close to the specimen surface which is the result of complex formation with glyoxylic acid. This explains the depletion of iron and aluminium in the PC acid-degraded layer shown in Table 6.

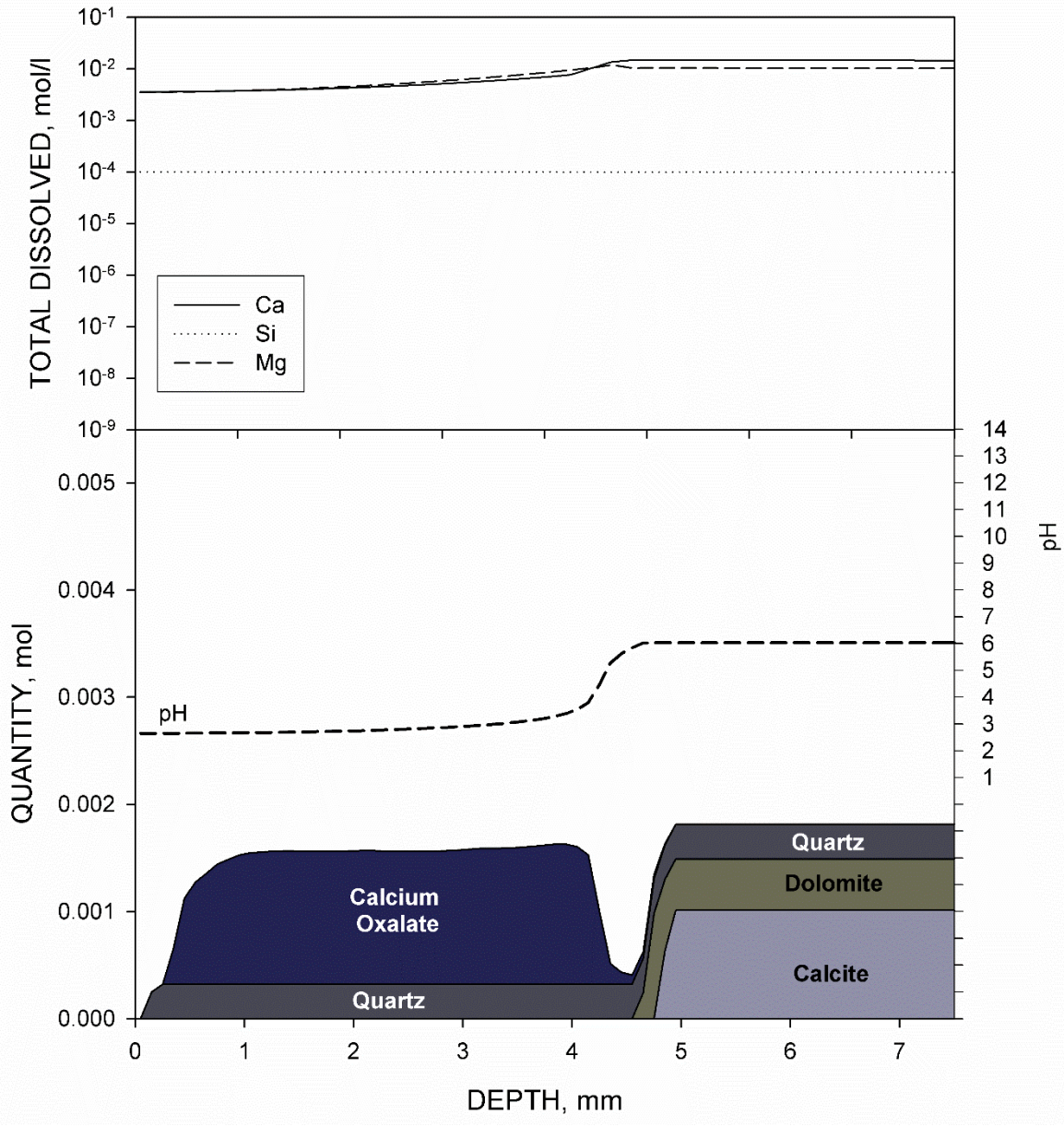

Figure 5. Results of geochemical modelling of glyoxylic acid attack on limestone, showing mineralogy and dissolved ions versus depth into the specimen.

The results from the CSA cement paste specimen model are shown in Figure 7. Two distinct layers resulting from exposure to acid are evident. The outermost of these comprises only calcium oxalate, beyond which is a layer consisting principally of gibbsite and calcium oxalate. A gibbsite-enriched layer of this type is often observed in CSA cement which has been exposed to acidic conditions. This results from the decomposition of calcium aluminate hydrates in the original hardened paste, followed by the precipitation of gibbsite. For instance, in the case of monosulfate:

$$Ca_4Al_2(SO_4)(OH)_{12}\cdot 6H_2O + 6H^+ \rightarrow 2Al(OH)_3 + SO_4^{2-} + 4Ca^{2+} + 12H_2O$$

The accumulation of gibbsite in the acid-degraded layers of hardened CSA cement paste exposed to acids progresses further due to the compound being soluble under acidic conditions, but highly insoluble at intermediate pH. At low pH, gibbsite dissolves and aluminium ions diffuse both towards and away from the cement surface. Ions diffusing towards the surface are released into the surrounding acid solution. However, ions diffusing inwards encounter higher pH conditions, leading to the re-precipitation of gibbsite (Scrivener et al. 1999). This accumulation was observed experimentally (along

with iron, which behaves similarly). In the case of glyoxylic acid, the dissolution of gibbsite is increased by the formation of complexes with aluminium, evidenced by the very high concentrations of this ion in solution, and the narrow width of the gibbsite-rich layer.

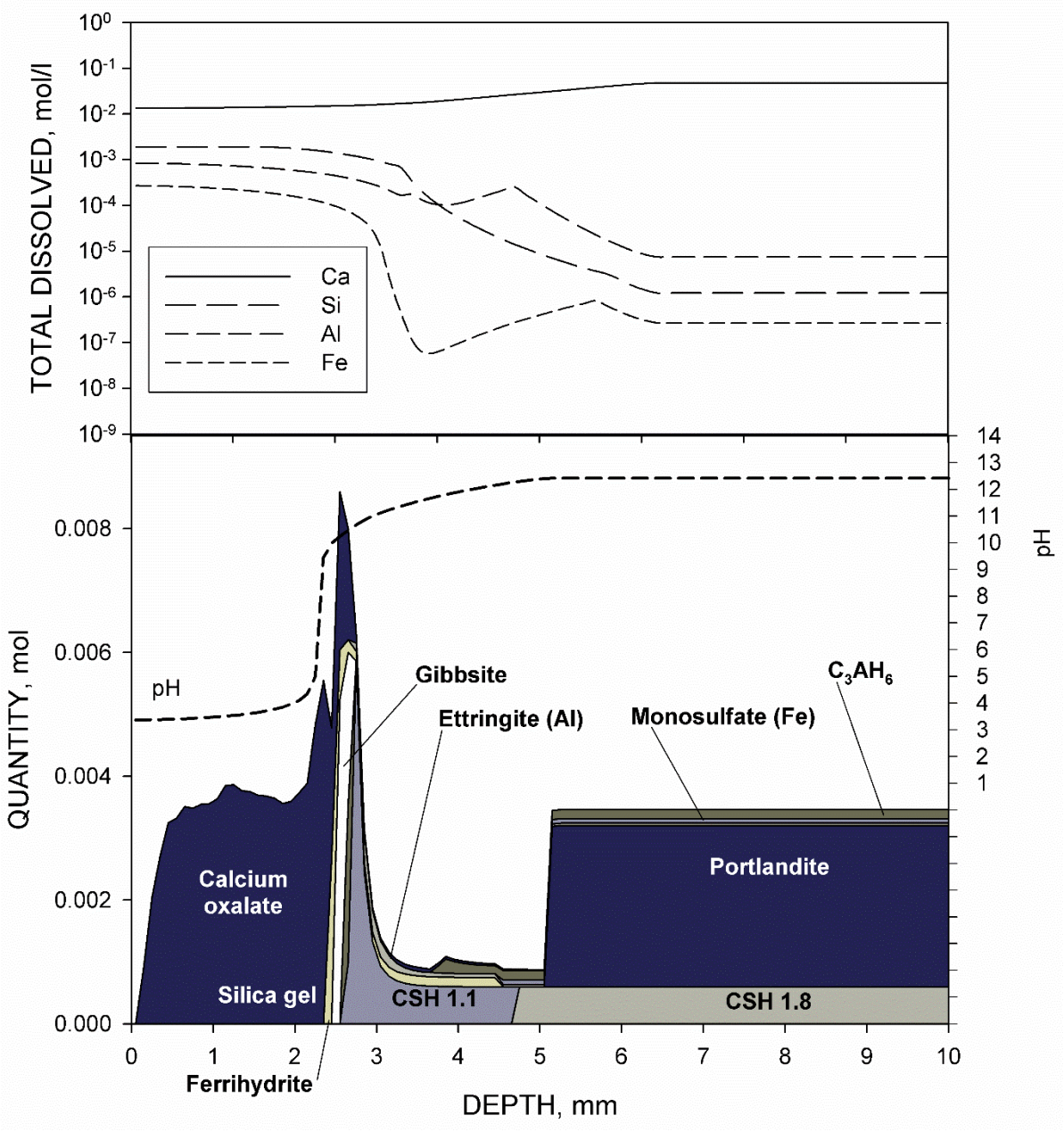

Figure 6. Results of geochemical modelling of glyoxylic acid attack on hardened PC cement paste, showing mineralogy and dissolved ions versus depth into the specimen.

The mineral composition of the gibbsite-rich layer observed in the model is essentially the same as that of the acid-degraded layer removed from the CSA specimen. It should be remembered that the CT scan of the CSA specimen showed a loss of material from the surface. According to the geochemical model, this would appear to be the result of the loss of the outer layer comprising only calcium oxalate. However, the analysis of the sediment in the CSA specimen tank identified both whewellite and gibbsite, suggesting that a proportion of gibbsite also falls away.

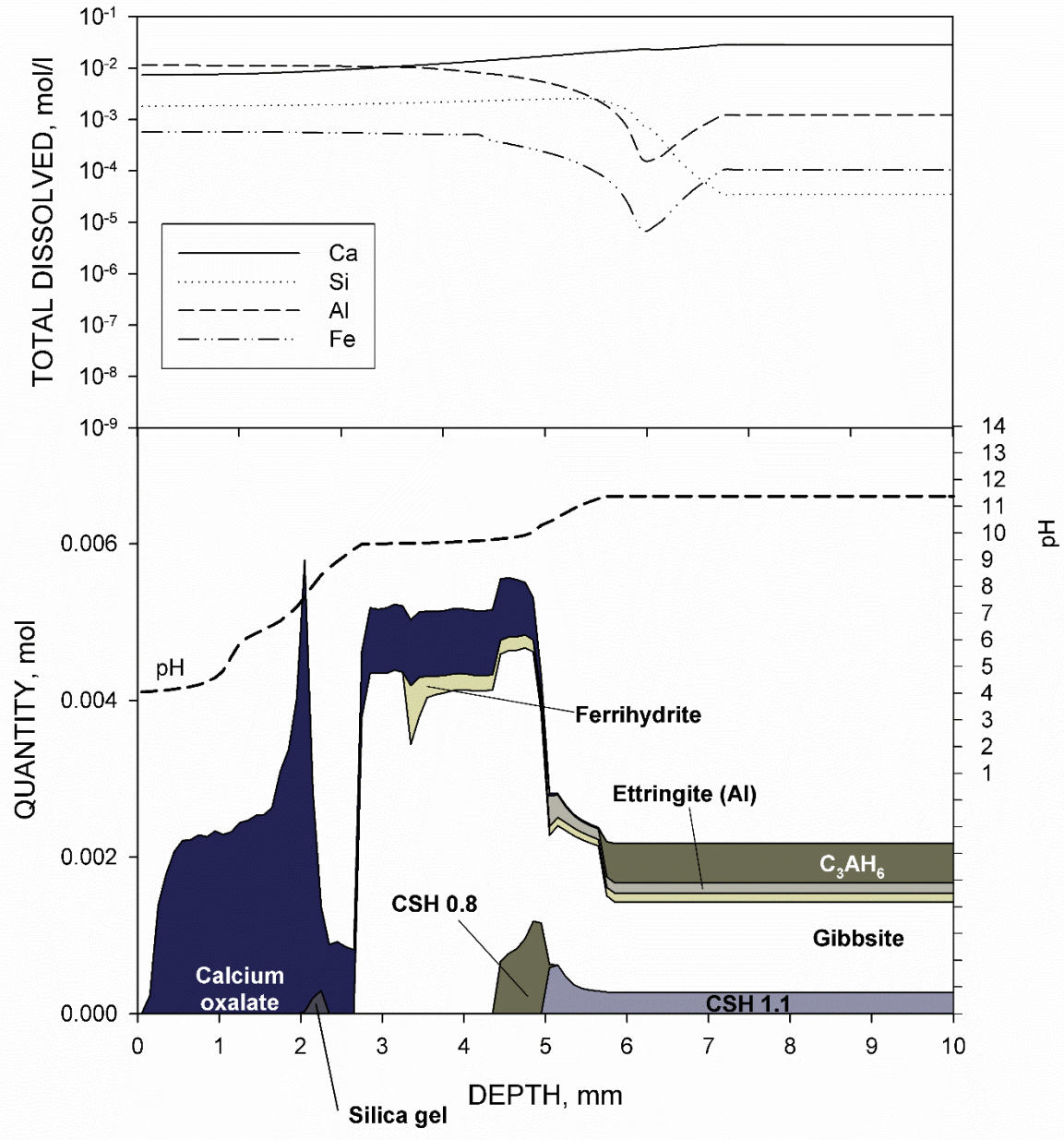

Figure 7. Results of geochemical modelling of glyoxylic acid attack on hardened CSA cement paste, showing mineralogy and dissolved ions versus depth into the specimen.

4. DISCUSSION

4.1 The Mechanism of Glyoxylic Acid Attack

Examination of the CT images indicate that the PC specimen was most susceptible to glyoxylic acid attack followed by CSA cement and then limestone. The sandstone specimen was seemingly wholly resistant to attack. Powder X-ray diffraction suggests that the grains of quartz in the sandstone specimen were cemented by feldspar and clay minerals, which are highly insoluble. It would be incorrect to conclude that all sandstones would be equally resistant, with those cemented with carbonate minerals such as calcite likely to be vulnerable to attack.

Whilst the synthesis of calcium glyoxylate proved to be of less relevance than initially anticipated, the results did yield useful information. Firstly, the results suggest that the conversion of glyoxylate ions to oxalate probably requires basic conditions. This is because the salt synthesised under neutral conditions

did not appear to convert to the calcium oxalate, whereas the synthesis involving a lime solution did. In both syntheses calcium ions were present in high quantities ruling out their role. The geochemical models developed in this paper assume that calcium glyoxylate is first precipitated, followed by a rapid conversion. However, it should be stressed that there is no direct evidence of this, and that conversion may occur in solution without any need for a calcium glyoxylate precursor.

Using the structural data discussed earlier, it can be determined that calcium glyoxylate has a molar volume of 126 cm^3 mol^{-1}. The molar volume of calcite is 37 cm^3 mol^{-1}, whilst the molar volume of portlandite in hydrated Portland cement is 33 cm^3 mol^{-1}. Thus, the reaction of either of these compounds to form calcium glyoxylate is likely to be expansive in nature. However, the seeming absence of solid calcium glyoxylate during glyoxylic acid attack – or at least its fleeting presence - means that it is unlikely that salt precipitation a deterioration mechanism. Moreover, the CT scans present no evidence of expansive damage, at least in the case of the cement specimens. Fragmentation of sorts was observed in the limestone specimen, but disintegration of limestone during weathering – even where salts are not formed - is common (Emmanuel and Levenson 2014).

From the above discussion, a single overall conclusion can be drawn: it would appear that glyoxylic acid derived from fungal degradation of bird excreta will attack calcium-based construction materials through a process of acidolysis, with complex formation between iron and aluminium ions providing a secondary deterioration mechanism where these elements are present. However, the chemistry of the system studied is notably more elaborate than most forms of organic acid attack, with multiple organic species being formed. The scheme by which glyoxylic acid reacts to form these other species is summarised in Figure 8, although other reactions may also occur. A key feature of this scheme is the formation of significant quantities of oxalic acid. The formation of this acid in bird excreta has already been noted in the introduction, although this has been attributed to bacterial activity (Hutchinson 1950). The results presented in this paper appear to show that there is an additional, partly abiotic, route: microbial degradation to glyoxylic acid followed by a reaction with mineral substrates to form oxalate. These substrates need not, of course, be buildings.

The increase in pH observed in the experiments is most probably the result of marked precipitation of calcium oxalate in the exposure solution. The introduction of a photooxidation process involving oxalate ions and glyoxal into the models adequately replicates the pH change. Whether this process – or a similar one – plays a role requires further investigation.

4.2 Occurrence of Oxalate Compounds on Stone and Concrete

The findings presented in this paper also have broader significance with regards to the biodeterioration of stone and concrete. The presence of calcium oxalate minerals at stone and concrete surfaces on which fungi have grown is extremely common. In some cases this is associated with deterioration (Angeles de la Torre et al. 1992; Fomina et al. 2005; Fomina et al. 2007), but in other cases, it has a protective effect (Ariño et al. 1995; Di Bonaventura et al. 1999; McIlroy de la Rosa et al. 2012). Indeed, applications based on oxalic acid are applied to calcium-bearing stone and concrete surfaces to create a protective coating (Voegel et al. 2015; Burgos-Cara et al. 2017). This effective because the calcium oxalate salts which precipitate have a volume slightly higher than the original calcite and/or portlandite crystals, blocking pores without creating sufficient stress to cause cracking.

Despite the precipitation of calcium oxalate in the experiments reported in this paper, a protective effect is not observed. This is because acid attack occurs first, followed by the formation of calcium oxalate salt. Thus, one possible explanation for deterioration observed in the presence of calcium oxalate is that oxalic acid formation by fungi is not the source of the damage. Instead, the deterioration derives from glyoxylic acid production, with calcium oxalates being a product of glyoxylate conversion.

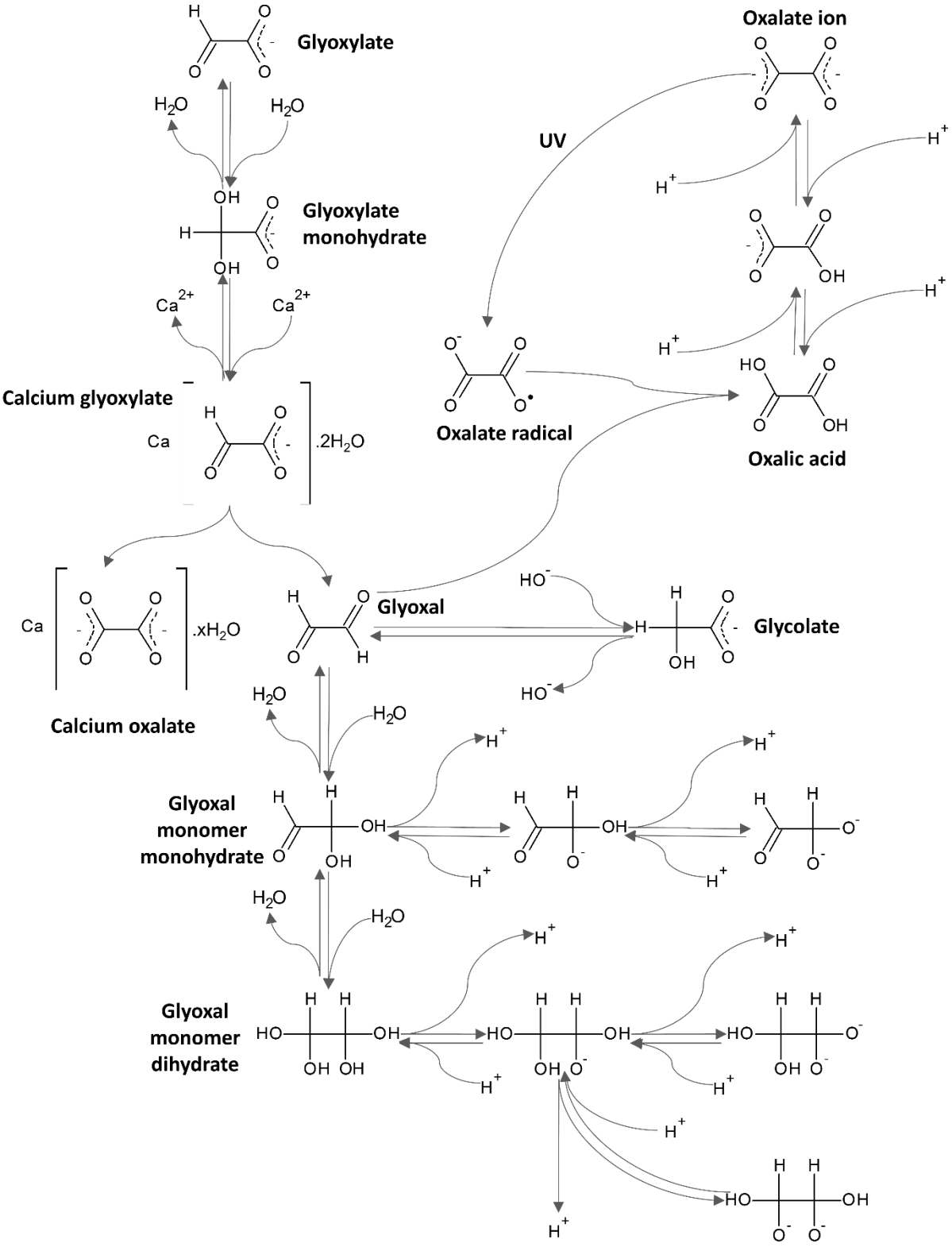

Figure 8. A reaction scheme for glyoxylic acid, showing the likely reactions effective during the experiments. Partly based on a scheme from Fratzke and Reilly (1986).

4.3 Estimating Biodeterioration Rates

The extent to which glyoxylic acid deriving from fungal decomposition of bird excreta is likely to act as a deteriorating agent needs to be considered in further detail.

A wide range of fungi are capable of degrading uric acid to glyoxylic acid, including several commonly encountered *Penicillium* and *Aspergillus* species (Vogels and Van der Drift 1976). This means that fungal degradation and glyoxylic acid production is a likely progression after deposition of bird excreta.

Previous research discussed in the introduction has clearly identified acid formation as a source of damage. However, the same research has also found that the drop in pH observed during decomposition is followed by a rise, indicating that attack from glyoxylic acid from excreta occurs within a limited timeframe. However, it must also be remembered that the deposition of bird excreta tends to be an ongoing process and, therefore, exposure to the acid has the potential to be sustained.

If the assumption is made that a given mass of glyoxylic acid can be directly related to volume lost from a surface, an estimate of damage from a volume of bird excreta is possible. If the degradation of uric acid by fungi is considered in a truncated form:

$$2C_5H_4N_4O_3 + 2H_2O + 3O_2 \rightarrow 2C_2H_2O_3 + 4CO(NH_2)_2 + 2CO_2$$

1 kg of uric acid is converted into 440 g of glyoxylic acid. Pigeon excreta is reported as containing up to 126 mg l^{-1} of uric acid (Harr 2002). Using this value, 1 litre of pigeon excreta - if fully degraded by fungi - would yield 55.4 mg of glyoxylic acid. Using the mass of glyoxylic acid contained within each tank at the beginning of the experiments (29.6 g) and the degraded volumes observed from micro-CT imaging - and assuming a linear correlation - 1 litre of pigeon excreta possesses the capacity to erode 10, 22 and 21 mm^3 of limestone, PC or CSA cement paste respectively. Whilst these quantities are relatively small, it must be noted that pigeons will produce 3 kg (dry mass) of excreta per year (Terres 1987), which equates to approximately 12 litres of wet matter. Thus, in urban environments, where thousands of birds may roost on one building, and given the long service lives expected of the built environment (typically > 40 years), the potential for significant damage is real.

Field studies of the attack of stone deriving from bird excreta have tended to be qualitative in nature, and so comparison of these estimated rates with field data is not possible. However, comparison with data relating to attack from acid rain is potentially meaningful. A study of limestone monuments exposed to acid rain in locations around the United States found maximum rates of 9 µm $year^{-1}$ in regions of high acid rain, with natural weathering conditions yielding rates of around half this (Meierding 1993). Assuming potential exposure to glyoxylic acid throughout a year to be 100 mg, an estimate based on the results of this study suggests a rate of recession of around 7 µm $year^{-1}$. It should also be noted that where other sources of acidity exist, such as acid rain, the effect of the presence of glyoxylic acid is likely to be additive with regards to the rate of weathering.

4.4 Limiting Damage from Pigeon Excreta

There are many reasons for limiting the extent to which bird excreta is deposited on buildings, including those of human health and aesthetics. However, the results of this paper and previous research clearly indicate that it possesses the potential to cause physical damage to stone and concrete, with calcium-based materials likely to be more vulnerable. In the case of existing buildings, measures to limit the extent to which birds settle on buildings are well-established. Moreover, approaches to limiting the acidity of pigeon excreta through controlling food sources that birds have access to have been proposed (Spennemann et al. 2017).

In the case of new buildings, selection of materials less prone to attack at locations which may encounter bird excreta is desirable. Protective coatings are also worth considering, although the lifetimes of these usually cover a shorter period than the service life of buildings. Where concrete and related materials, such as mortar, are used, there exists the option of proportioning constituents such that resistance is enhanced. It has already been seen that calcium aluminate cements have a slight advantage over Portland cement in resisting glyoxylic acid attack. Given that the mode of deterioration of cement by glyoxylic acid is acidolysis, an alternative approach is the combination of Portland cement with pozzolanic materials such as fly ash or latent hydraulic materials such as GGBS. This approach works

because it limits the levels of portlandite present, whose dissolution is most immediate and which leads to a significant loss in strength (Dyer 2017). The use of calcareous aggregate may provide a means of further neutralising the acid. However, a reduced water / cement ratio - which will limit mass transport rates through concrete – is likely to offer the best means of resisting attack.

5. CONCLUSIONS

Glyoxylic acid, which is produced by the fungal degradation of bird excreta, has been shown to attack limestone and cement through a process of acidolysis. The acid also forms strong complexes with iron and aluminium, which increases the rate of dissolution of these elements.

During attack, glyoxylate ions react to form oxalate ions, resulting in the precipitation of calcium oxalate. Where calcium-based building materials are likely to encounter bird excreta, measures to limit the rate of deterioration are advisable.

6. ACKNOWLEDGEMENTS

The author would like to thank Ms Lisha Tan for assistance with the experimental work reported in this paper. The author also wishes to acknowledge the use of the EPSRC-funded National Chemical Database Service hosted by the Royal Society of Chemistry.

7. REFERENCES

Adu-Wusu, K., 2012. Literature review on impact of glycolate on the 2H evaporator and the effluent treatment facility (ETF). Savannah River National Laboratory, Aiken.

Angeles de la Torre, M., Gomez-Alarcon, G., Vizcaino, C., Teresa Garcia, M., 1992. Biochemical mechanisms of stone alteration carried out by filamentous fungi living in monuments. Biogeochemistry 19, 129–147.

Ariño, X., Ortega-Calvo, J.J., Gomez-Bolea, A., Saiz-Jimenez, C., 1995. Lichen colonization of the Roman pavement at Baelo Claudia (Cadiz, Spain): biodeterioration vs. bioprotection. Science of the Total Environment 167, 353-363.

Arnórsson, S., Stefánsson, A., 1999. Assessment of Feldspar solubility constants in water in the range of 0 °C to 350 °C at vapor saturation pressures. American Journal of Science 299, 173-209.

Bachrach, U., 1957. The aerobic breakdown of uric acid by certain pseudomonads. Journal of General Microbiology 16, 1-11.

Bassi, M., Chiatante, D., 1976. The role of pigeon excrement in stone biodeterioration. International Biodeterioration Bulletin 12, 73-79.

Berg, W., Hesse, A., Schneider, H.-J., 1976. A contribution to the formation mechanism of calcium oxalate urinary calculi. III. On the role of magnesium in the formation of oxalate calculi. Urological Research 4, 161–167.

Bernardi, E., Bowdem, D.J., Brimblecombe, P., Kenneally, H., Morselli, L., 2009. The effect of uric acid on outdoor copper and bronze. Science of the Total Environment 407, 2383-2389.

British Standards Institution, 2011. EN 197-1:2011 Cement. Composition, specifications and conformity criteria for common cements. British Standards Institution, London, UK.

Burgos-Cara, A., Ruiz-Agudo, E., Rodriguez-Navarro, C., 2017. Effectiveness of oxalic acid treatments for the protection of marble surfaces. Materials and Design 115, 82–92.

804 Carde, C., François, R., 1997. Effect of the leaching of calcium hydroxide from cement paste on
805 mechanical and physical properties. Cement and Concrete Research 27, 539-550.

806 Carlile, F.S., 1984. Ammonia in poultry houses: a literature review. World's Poultry Science Journal 40,
807 99-113.

808 Carlton, A.G., Turpin, B.J., Altieri, K.E., Seitzinger, S., Reff, A., Lim, H.-J., Ervens, B., 2007. Atmospheric
809 oxalic acid and SOA production from glyoxal: results of aqueous photooxidation experiments.
810 Atmospheric Environment 41, 7588–7602.

811 Chapman, D.V., 1996. Water Quality Assessments: A guide to the use of biota, sediments and water in
812 environmental monitoring, 2nd ed. Taylor and Francis, London.

813 Christodoulou, E., Panias, D., Paspaliaris, I., 2001. Calculated solubility of trivalent iron and aluminum in
814 oxalic acid solutions at 25°C. Canadian Metallurgical Quarterly 40, 421-432.

815 Debus, H., 1904. Contributions to the history of glyoxylic acid. Journal of the Chemical Society,
816 Transactions 85, 1382-1403.

817 Del Monte, M., 1986. Chemical and biological weathering of an historical building: Reggio Emilia
818 Cathedral. Science of the Total Environment 50, 165-182.

819 De Windt, L., Devillers, P., 2010. Modeling the degradation of Portland cement pastes by biogenic
820 organic acids. Cement and Concrete Research 40, 1165–1174.

821 Di Bonaventura, M.P., Del Gallo, M., Cacchio, P., Ercole, C., Lepidi, A., 1999. Microbial formation of
822 oxalate films on monument surfaces: bioprotection or biodeterioration? Geomicrobiology Journal 16,
823 55-64.

824 Dyer, T.D., 2017. Influence of cement type on resistance to attack from two carboxylic acids. Cement
825 and Concrete Composites 83, 20-35.

826 Emmanuel, S., Levenson, Y., 2014. Limestone weathering rates accelerated by micron-scale grain
827 detachment. Geology 42, 751-754.

828 Fomina, M.O., Olishevska, S.V., Kadoshnikov, V.M., Zlobenko, B.P., Pidgorsky, V.S., 2005. Concrete
829 colonization and destruction of mitosporic fungi in model experiment. Mikrobiolohichnyĭ Zhurnal 67,
830 96-104.

831 Fomina, M., Podgorsky, V.S., Olishevska, S.V., Kadoshnikov, V.M., Pisanska, I.R., Hillier, S., Gadd, G.M.,
832 2007. Fungal deterioration of barrier concrete used in nuclear waste disposal. Geomicrobiology Journal
833 24, 643-653.

834 Forouzan, F., Richards, T.C., Bard, A.J., 1996. Photoinduced reaction at TiO_2 particles. Photodeposition
835 from Ni II solutions with oxalate. Journal of Physical Chemistry 100, 18123-18127.

836 Fratzke, A.R., Reilly, P.J., 1986. Kinetic analysis of the disproportionation of aqueous glyoxal.
837 International Journal of Chemical Kinetics 18, 757-773.

838 Giordani, P., Modenesi, P., Tretiach, M., 2003. Determinant factors for the formation of the calcium
839 oxalate minerals, weddellite and whewellite, on the surface of foliose lichens. Lichenologist 35, 255–
840 270.

841 Glasser, F.P., 1992. Chemistry of cement-solidified waste forms. In: Spence, R.D. (Ed.), Chemistry and
842 Microstructure of Solidified Waste Forms. Lewis Publishers, Boca Raton, pp. 1-39.

843 Gómez-Heras, M., Benavente, D., Álvarez de Buergo, M., Fort, R., 2004. Soluble salt minerals from
844 pigeon droppings as potential contributors to the decay of stone based Cultural Heritage. European
845 Journal of Mineralogy 16, 505-509.

846 Haag-Wackernagel, D., 2012. Straßentauben am gebäude – probleme und lösungen. In: Zwiener, G.,
847 Lange, F.-M. (Eds.), Handbuch Gebäude-Schadstoffe und Gesunde Innenraumluft, Schmidt Verlag,
848 Berlin, pp. 527-633.

849 Hancock, R.D., Martell, A.E., 1989. Ligand design for selective complexation of metal ions in aqueous
850 solution. Chemical Reviews 89, 1875-1914.

851 Harr, K.E., 2002. Clinical chemistry of companion avian species: A review. Veterinary Clinical Pathology
852 31, 140-151.

853 Hempel, K., Moncrieff, A., 1971. Summary of work on marble conservation at the Victoria and Albert
854 Museum conservation department up to August 1971. In: Rossi-Manaresi, R., Torraca, G. (Eds.), The
855 Treatment of Stone: Proceedings of the Meeting of the Joint Committee for the Conservation of Stone,
856 Bologna, October 1-3, 1971, Centro per la Conservazione delle Sculture all'Aperto, Bologna, pp. 165-
857 182.

858 Hutchinson, G.E., 1950. Survey of Existing Knowledge of Biogeochemistry. 3. The Biogeochemistry of
859 Vertebrate Excretion. Bulletin of the American Museum of Natural History 96. American Museum of
860 Natural History, New York.

861 Joint Chemical and Pharmaceutical Company, 2017. Product List. Joint Chemical and Pharmaceutical
862 Company, Moscow, online at
863 **{** HYPERLINK "http://www.chembuyersguide.com/images/novochem.pdf" **}**

864 Larreur-Cayol, S., Bertron, A., Escadeillas, G., 2011. Degradation of cement-based materials by various
865 organic acids in agro-industrial waste-waters. Cement and Concrete Research 41, 882–892.

866 Lisci, M., Monte, M., Pacini, E., 2003. Lichens and higher plants on stone: a review. International
867 Biodeterioration and Biodegradation 51**,** 1–17.

868 Lothenbach, B., Matschei, T., Möschner, G., Glasser, F.P., 2008. Thermodynamic modelling of the effect
869 of temperature on the hydration and porosity of Portland cement. Cement and Concrete Research 38,
870 1–18.

871 Malik, M., Joens, J.A., 2000. Temperature dependent near-UV molar absorptivities of glyoxal and
872 gluteraldehyde in aqueous solution. Spectrochimica Acta Part A 56, 2653-2658.

873 Manissorn, K., Fong-ngern, K., Peerapen, P., Thongboonkerd, V., 2017. Systematic evaluation for effects
874 of urine pH on calcium oxalate crystallization, crystal-cell adhesion and internalization into renal tubular
875 cells. Scientific Reports 7, article number: 1798.

876 Martell, A.E., Smith, R.M., 2001. Critical Selected Stability Constants of Metal Complexes Database,
877 Version 6.0 for Windows; National Institute of Standards and Technology, online at
878 **{** HYPERLINK "https://www.nist.gov/srd/nist46" **}**

879 McIlroy de la Rosa, J.P., Warke, P.A., Smith, B.J., 2012. Lichen-induced biomodification of calcareous
880 surfaces: bioprotection versus biodeterioration. Progress in Physical Geography 37, 325–351.

881 Meierding, T.C., 1993. Inscription legibility method for estimating rock weathering rates.
882 Geomorphology 6, 273-286.

883 Montoya, M.R., Mellado, J.M.R., 1995. Hydration constants of carbonyl and dicarbonyl compounds:
884 comparison between electrochemical and no electrochemical technique. Portugaliae Electrochimica
885 Acta 13, 299–303.

886 Öhman, L.O., Nordin, A., Sedeh, I.F., Sjöberg, S., 1991. Equilibrium and structural studies of silicon(IV)
887 and aluminium(III) in aqueous solution. 28. Formation of soluble silicic acid–ligand complexes as studied
888 by potentiometric and solubility measurements. Acta Chemica Scandinavica 45, 335–341.

889 Okochi, H., Brimblecombe, P., 2002. Potential trace metal–organic complexation in the atmosphere. The
890 Scientific World 2, 767–786.

Parkhurst, D.L., Appelo, C.A.J., 2013. Description of input and examples for PHREEQC version 3 – A computer program for speciation, batch-reaction, one-dimensional transport, and inverse geochemical calculations. In: U.S. Geological Survey Techniques and Methods, Book 6, Chapter A43. US Geological Survey, Denver, online at
{ HYPERLINK "https://pubs.usgs.gov/tm/06/a43/" }

Reesman, A.L., Keller, W.D., 1965. Calculation of standard free energies of formation of six rock-forming silicate minerals from solubility data. American Mineralogist 50, 1729-1739.

Schweitzer, F., Magi, L., Mirabel, P., George, C., 1998. Uptake rate measurements of methanesulfonic acid and glyoxal by aqueous droplets. Journal of Physical Chemistry 102, 593-600.

Scrivener, K.L., Cabiron, J.-L., Letourneux, R., 1999. High-performance concretes from calcium aluminate cements. Cement and Concrete Research 29, 1215–1223.

Smith, J.T., Doctor, V.M., 1975. Properties of binary complexes between metal ions and glyoxalic or alphaketoglutaric or imidazolypyruvic acid. Journal of Inorganic and Nuclear Chemistry 37, 775-777.

Spennemann, D.H.R., Pike, M., Watson, M.J., 2017. Effects of pigeon excreta on building conservation. International Journal of Building Pathology and Adaption 35, 2-15.

Stanga, M., 2010. Sanitation: Cleaning and Disinfection in the Food Industry. Wiley-VCH, Weinheim.

Streit, J., Tran-Ho, L.C., Koenigsberger, E., 1998. Solubility of calcium oxalate hydrates in sodium chloride solutions and urine-like liquors. Monatshefte für Chemie 129, 1225-1236.

Stronach, S.A., Glasser, F.P., 1997. Modeling the impact of abundant geochemical components on phase stability and solubility of the $CaO–SiO_2–H_2O$ systems at 25 °C: Na^+, K^+, SO_4^{2-}, Cl^- and CO_3^{2-}. Advances in Cement Research 9, 167–181.

Tanaka, S., Kageyama, H., Ono, H., Kuruma, A., 2010. Crosslinking agent, crosslinked polymer, and uses thereof. Patent number US20100209723 A1.

Terres, J.K., 1987. The Audobon Society Encyclopedia of North American Birds. Alfred A Knopt, New York.

Topal, T., Sözmen, B., 2003. Deterioration mechanisms of tuffs in Midas monument. Engineering Geology 68, 201-223.

U.S. Environmental Protection Agency, 1999. MINTEQA2/PRODEFA2, A geochemical assessment model for environmental systems—User manual supplement for version 4.0. National Exposure Research Laboratory, Athens, GA.

Vera-Ponce de Leon, A., Sanchez-Flores, A., Rosenblueth, M., Martinez-Romero, E., 2016. Fungal community associated with *Dactylopius* (Hemiptera: Coccoidea: Dactylopiidae) and its role in uric acid metabolism. Frontiers in Microbiology 7, article 954.

Vincze, L., 1999. Determination of stability constants and individual quantum yields of iron (III) - glyoxylate complexes. Hungarian Journal of Industrial Chemistry 27, 241-244.

Voegel, C., Bertron, A., Erable, B., Escadeillas, G., 2015. Chemical treatment with oxalic acid to improve the durability of cement-based materials in acid environment. In: Quattrone, M., John, V.M. (Eds.), XIII International Conference on Durability of Building Materials and Components - XIII DBMC. RILEM, Paris, pp. 670-678.

Vogels, G.D., Van der Drift, C., 1976. Degradation of purines and pyramidines by microorganisms. Bacteriological Reviews 40, 403-468.

Weast, R.C., Astel, M.J., Beyer, W.H., 1986. CRC Handbook of Chemistry and Physics (67^{th} ed.). CRC Press, Boca Raton.

Wojdyr, M., 2010. Fityk: a general-purpose peak fitting program. Journal of Applied Crystallography 43, 1126-1128.

Zepp, R.G., Faust, B.C., Hoigné, J., 1992. Hydroxyl radical formation in aqueous reactions (pH 3-8) of iron (II) with hydrogen peroxide: the photo-Fenton reaction. Environmental Science and Technology 26, 313-319.

Ziogos, A.D., Brown, M.J., Ivanovic, A., Morgan, N., 2015. Interface shear characteristics of Scottish rock samples from sites with tidal energy potential. In: Winter, M.G., Smith, D.M., Eldred, P.J.L., Toll D.G. (Eds.), Proceedings of the XVI ECSMGE Geotechnical Engineering for Infrastructure and Development. ICE Publishing, London, pp. 1357-1362.

Funding

This research did not receive any specific grant from funding agencies in the public, commercial, or not-for-profit sectors.